PCCP

PAPER

View Article Online
View Journal

Cite this: DOI: 10.1039/c6cp03170f

Polarization-driven catalysis *via* ferroelectric oxide surfaces†

Arvin Kakekhani*[abcd] and Sohrab Ismail-Beigi*[abef]

Received 10th May 2016,
Accepted 28th June 2016

DOI: 10.1039/c6cp03170f

www.rsc.org/pccp

The surface chemistry and physics of oxide ferroelectric surfaces with a fixed polarization state have been studied experimentally for some time. Here, we discuss the possibility of using these materials in a different mode, namely under cyclically changing polarization conditions achievable *via* periodic perturbations by external fields (*e.g.*, temperature, strain or electric field). We use Density Functional Theory (DFT) and electronic structure analysis to understand the polarization-dependent surface physics and chemistry of ferroelectric oxide $PbTiO_3$ as an example of this class of materials. This knowledge is then applied to design catalytic cycles for industrially important reactions including NO_x direct decomposition and SO_2 oxidation into SO_3. The possibility of catalyzing direct partial oxidation of methane to methanol is also investigated. More generally, we discuss how using ferroelectrics under cyclically changing polarization conditions can help overcome some of the fundamental challenges facing the catalysis community such as the limitations imposed by the Sabatier principle and scaling relations.

1. Introduction

Surface catalysis based on transition metals and their alloys has been one of the most important research fields in theoretical and experimental catalysis and chemistry.[1–4] In addition to basic scientific discoveries, this field has had enormous impacts on daily lives, *e.g.*, it has helped overcome the world hunger problem by introducing the Haber–Bosch process to synthesize ammonia.[5–7] A significant breakthrough for transition metal catalysis in the last few decades has been the introduction of a predictive theory for catalysis based on a combination of the d-band model, activity maps and scaling relations.[8] In addition to helping transform heterogeneous catalysis from a trial-and-error approach to a controlled design process[8–10] and enabling the design of more effective catalysts for important reactions,[3,11,12] this theory has identified some of the fundamental limitations of current catalytic methods and materials.[8,9,13] These limitations stem from the strong correlations among the binding energies of reactants, intermediates and products (known as scaling relations[14–26]) which make it challenging to design a surface that has an optimum surface–adsorbate interaction as dictated by the Sabatier principle:[27,28] a surface–adsorbate interaction that is neither too strong to limit the catalytic activity by desorption of products nor too weak to limit it by adsorption of the reactants. The optimum is the apex of the ubiquitous "volcano plots"[10,14] of catalytic activity maps. However, scaling relations restrain us from getting close enough to this maximum catalytic activity.[9,13,29]

There are two possible solutions to the fundamental problem mentioned above. First, one can continue to work within the framework of the Sabatier principle (*i.e.*, using surfaces with fixed surface chemistry) and try to fabricate surfaces and materials that break the usual scaling relations[30–32] or obey a different set of these relations which move one closer to the optimum surface–adsorbate interaction (this approach has proven challenging thus far). Second, one can break away from the Sabatier principle and use surfaces with dynamic and controllable surface chemistry which enables one to periodically enhance adsorptive and desorptive behaviors on a surface rather than compromising for a single optimized interaction strength.[33,34]

The first approach has recently been reviewed by Norskov and Vojvodic.[9] Separately, we explained the second approach[33–35] by theoretically designing catalytic cycles driven by the switchable polarization of ferroelectrics to catalyze important reactions including water splitting.[35] A new theoretical study has applied this idea to CO_2 dissociation process.[36] In this paper, we will mainly focus on the use of ferroelectrics in the framework of going beyond the Sabatier principle.[34] However, we mention an

[a] Department of Physics, Yale University, New Haven, CT 06520, USA. E-mail: sohrab.ismail-beigi@yale.edu
[b] Center for Research on Interface Structure and Phenomena (CRISP), Yale University, New Haven, CT 06520, USA
[c] Department of Chemical Engineering, Stanford University, Stanford, CA 94305, USA. E-mail: kake@stanford.edu
[d] Center for Interface Science and Catalysis (SUNCAT), Stanford University, Stanford, CA 94305, USA
[e] Department of Applied Physics, Yale University, New Haven, CT 06520, USA
[f] Department of Mechanical Engineering and Materials Science, Yale University, New Haven, CT 06520, USA

† Electronic supplementary information (ESI) available. See DOI: 10.1039/c6cp03170f

example that shows how ferroelectrics might be potentially useful for breaking away from current scaling relations. We believe this is an intriguing example which points to future research.

Since the 1950s, the catalytic properties of ferroelectric surfaces have been experimentally studied.[33,37–45] For example, it has been shown that by using ferroelectric-based materials one can achieve polarization-dependent and enhanced photocatalysis[46–66] due to internal fields that improve electron–hole separation.[46–56,67–70] Ferroelectric polarization can also affect molecular adsorption onto and desorption from surfaces.[38,71–83] Ferroelectric materials are also both piezoelectric and pyroelectric[53,84–89] which means that their polarization is coupled to both strain[90–98] and temperature fields (in addition to electric fields). Since 2010, the uses of piezoelectric and pyroelectric properties to achieve catalytic activity under dynamic external fields (strain or temperature) have been experimentally explored[99–110] and the terms "piezoelectrochemical effect" and "pyroelectrocatalysis" have been coined. In tandem with experimental studies, the continued development of computational methods and facilities has made *ab initio* studies of ferroelectric surface chemistry possible.[77,79,111–120] Although the beyond-Sabatier theory is rather new[34] and, to the best of our knowledge, a direct experimental verification has not been reported yet, indirect evidence of the feasibility of the proposed ferroelectric cycles comes from the above piezoelectrochemical and pyroelectrocatalytic experiments.

In previous work on NO_x direct decomposition, the surface system consisted of a monolayer of active transition metal (*e.g.*, CrO_2 or RuO_2) on ferroelectric $PbTiO_3$.[34] In this work, we consider a simpler system that is easier to fabricate and study experimentally: the (001) surface of bare ferroelectric $PbTiO_3$. We investigate the behavior of this surface under cyclic polarization conditions for which the surface chemical properties can periodically alternate between oxidizing, inert and reducing behavior. We show that such a cycle can achieve NO_x direct decomposition at low coverages ($\leq$0.25 ML). We also show such a cycle can oxidize SO_2 into SO_3, the rate limiting step in the contact process which is the current major method for industrial production of sulfuric acid.[121,122] Lastly, the possibility of using ferroelectric oxides to catalyze the direct partial oxidation of methane to methanol is investigated as well. Methane (CH_4) is the major constituent of natural gas which is currently the cheapest source of hydrocarbons.[123] Developing a catalyst for the direct conversion of methane to (more valuable) methanol has been a major challenge in chemistry over the last decades[123–134] and has at times been called "a holy grail in catalytic sciences".[135]

In this paper, we study the surface chemistry of $PbTiO_3$(001) as a representative of the larger family of ferroelectric oxides.[136,137] We believe our results can be extended to other ferroelectric oxides (including $PbZr_xTi_{1-x}O_3$ or $BaTiO_3$ solid solutions[95,138–143]) since the polarization-dependent surface chemistry is not controlled by the exact type of atoms on the surface but the magnitude and sign of the ferroelectric polarization perpendicular to the surface which in turn dictates the doped surface charge.[33–35] We examine Pb terminated (001) $PbTiO_3$ because our calculations show that a Pb-terminated (as opposed to Ti terminated) surface is always more thermodynamically stable[144–147] in agreement with the experimental and theoretical literature.[35,117,148–151]

We note that the effect of surface polarization on surface catalytic properties and chemistry has been confirmed in other classes of materials.[152–166] For example, Bai *et al.* have recently shown that the surface polarization in Pt overlayers on Pd (stemming from the difference of electronegativity of two materials) leads to enhanced hydrogen evolution activity.[155,156] What makes ferroelectrics special is not merely the existence of a surface polarization but the fact that the polarization is a switchable order parameter[167–172] that couples to external fields.[33]

We note that one reason we choose to study the polarization dependent chemistry of a ferroelectric oxide, rather than another type of ferroelectric,[173–177] is that oxygen activity on ferroelectric oxide surfaces can be tuned by the polarization which permits one to drive reduction or oxidation reactions effectively.[35] We believe that the possibility of using the polarization dependent chemistry of other classes of ferroelectrics to drive surface reactions is an intriguing direction for future work.

2. Computational methods

We perform DFT calculations[178,179] with plane-wave basis sets using the Quantum Espresso software[180] together with ultrasoft pseudopotentials.[181–183] A slab geometry with the (001) surface normal and polarization axis is employed.[34,117] We introduce at least 15 Å of vacuum to isolate periodic copies of the slabs. A dipole correction in the center of the vacuum is used in order to eliminate the artificial electrical field and the unphysical dipole–dipole interactions among the copies of the slab in the z direction.[184] The plane-wave energy cutoff is 30 Ry. The k-sampling density of the Brillouin zone is 8×8 for a 1×1 primitive surface unit cell. The occupations of the Kohn–Sham states are smoothed using the cold smearing method of Marzari and Vanderbilt with a smearing width of 5 mRy/k_B.[185] The convergence criterion is that all atomic forces be smaller than 1×10^{-3} Ry Bohr^{-1}. The convergence threshold on stress for variable cell calculations is 0.5 kBar. In each ionic relaxation step, the energy convergence threshold for self-consistency is 1×10^{-6} Ry (in the final steps, close to the energy minimum, this value is automatically reduced by a factor of 100). These convergence parameters yield binding energies precise to better than 0.1 eV. The energies reported here are obtained using the GGA-PW91 exchange–correlation (XC) functional.[186,187] However, the main findings are checked to be independent of the specific choice of XC functional (for details see ESI†).

For the most part, we use $c(2 \times 2)$ in-plane periodicity for the supercell calculations, except if otherwise noted or in the case of simulations of lower adsorbate coverages ($\leq$0.25 ML). The $c(2 \times 2)$ structures have in-plane periodicity in the xy plane with a square unit cell with lattice constant 5.459 Å to model epitaxial growth on a $SrTiO_3$ substrate.[111,117] (This lattice constant for 2×2 structures is 7.72 Å.) We use a standard method whereby a few layers of Pt are placed on the bottom PTO surface to create an electrode with a large density of states at the Fermi level in

order to simulate an electron reservoir that would exist in a realistic thick ferroelectric film[34,114,117,188,189] (see ESI† for a sample supercell). Rather than simulating the effect of this physically relevant electron reservoir which would require extremely thick (and defective) ferroelectric films, the use of Pt layers allows us to simulate a thin and clean ferroelectric while not changing the surface chemistry on the opposite side of the ferroelectric slab. It should be noted that Pt layers have a small enough lattice mismatch (<4%) with the PTO slab so as not to introduce any artificial interface effect on the bottom PTO surface. We fix the structure of the second, third and fourth atomic layers of PTO on top of the Pt electrode to their bulk values in order to simulate the mechanical boundary conditions appropriate to a thick PTO film: this leads to reasonable computational expenses and sizes of the simulation cells.[34,117] As may be noticed below, the surface structure of positively polarized PTO surface experiences a geometric reconstruction which consists of surface Pb cations sliding in-plane by 0.5 unit cell, the reason for this behavior is discussed in the ESI.† Finally, we use the nudged elastic band (NEB)[190–193] and constrained relaxation[194,195] methods to calculate the energy barriers and transition states.[196,197]

The magnitude of polarization in bulk PTO is computed using the Berry phase method[198,199] to be $\approx$120.9 μC cm^{-2} for the PW91 GGA XC functional. As shown in prior work,[35] the magnitude of the polarization can be controlled in the simulation in order to study the surface chemistry as a function of polarization magnitude for each polarization direction: lowering the magnitude of the polarization smoothly transforms the surface chemistry from polar (either positive or negative) to non-polar (paraelectric) surface chemistry. The experimental value of polarization measured for PZT[200,201] is $\approx$90 μC cm^{-2}, but the surface chemistry predicted by $P \approx$ 120.9 μC cm^{-2} closely follows that of $P \approx$ 90 μC cm^{-2}.[35] A short discussion on how we control the polarization of the material is given in the ESI.†

3. Results and discussion

3.1. Switchable surface properties: oxidizing, reducing or inert

Similar to previous work on metal oxide monolayers (CrO_2 or RuO_2) on ferroelectric $PbTiO_3$,[34] our DFT calculations show a significant polarization dependent chemistry for the bare $PbTiO_3$ (PTO) surface. As it can be seen in Table 1, the direction and magnitude of the polarization can switch the surface chemistry from oxidizing (polarization pointing away from the surface, *i.e.*, negative direction) to inert (zero polarization) and to reducing (polarization pointing into the surface, *i.e.*, positive direction). On a positively polarized sample, the oxygen vacancy formation cost is high while oxygen atoms bind strongly to the surface. On a negatively poled surface, both the oxygen vacancy formation and atomic oxygen binding energies are negative: this means the stoichiometric negatively polarized surface not only desorbs oxygen atoms but tends to give away (0.5 ML) of its stoichiometric oxygen content.[35] In the paraelectric phase, the high oxygen vacancy formation energy together with a negative oxygen binding energy means a lack of interest for oxygen adsorption: the surface is inert. It should be noted that throughout this work, more positive numbers for binding energies indicate stronger binding since our chemisorption energy is defined as $E_{binding}$ = E(adsorbate) + E(surface) − E(adsorbate/surface).

Table 1 Polarization dependent atomic oxygen binding energy and oxygen vacancy formation energy (in 0.5 ML coverage) on stoichiometric Pb terminated $PbTiO_3$. Energies are relative to gas phase oxygen (*i.e.*, O in an O_2 molecule). More positive numbers for binding energies indicate stronger bonding, since our chemisorption energy is defined as $E_{binding}$ = E(adsorbate) + E(surface) − E(adsorbate/surface). The magnitude of polarization for both positive and negative cases is the polarization predicted by GGA-PW91 XC ($\approx$120 μC cm^{-2})

Polarization	Oxygen vacancy formation energy (eV)	Atomic oxygen binding energy (eV)
Positive	3.9	3
Paraelectric	3.7	−0.7
Negative	−0.7	−0.7

The surface chemistry is driven by the change in the surface compensating charge induced by the ferroelectric polarization $\vec{P}$ with areal charge density $\sigma = -\vec{P}\cdot\hat{n}$ where $\hat{n}$ is the surface unit normal vector.[33] When the compensating charge takes the form of electronic occupation of surface bands, this is known as an electronic reconstruction.[33,35,202–206] As can be seen in Fig. 1, electrons or holes are doped into the conduction or valence bands of the surface in positively or negatively poled surface, respectively. This polarization-dependent doped surface charge is the driving force behind the (polarization-dependent) surface chemistry.[35]

3.2. Catalysis using cyclic polarization modulation

In a cyclic scheme in which the magnitude and/or direction of the polarization is periodically changed by application of external fields (including electric fields, strain, or temperature individually or in combinations), one can exploit a combination of different surface chemistries (oxidizing, inert or reducing) and use each to efficiently drive different parts of an overall reaction.[34,35] In fact, we are going to use the strong

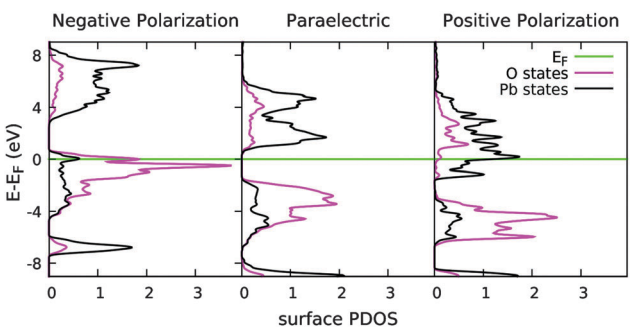

Fig. 1 Projected Density of States (PDOS) on surface Pb and O atoms on Pb-terminated $PbTiO_3$. As a result of ferroelectric polarization perpendicular to the surface, electrons or holes are doped into the surface conduction (dominated by Pb 6p states) or valence (dominated by O 2p states) bands in positively or negatively poled surfaces, respectively.

thermodynamic drive of the ferroelectric surface towards stabilizing reconstructions[33,112,115,116,151,207,208] to run the various reactions.[34,35] For this reason, we will be focusing on the behavior of stoichiometric surfaces in order to see how the dynamic process whereby the stoichiometry changes towards the final and stable reconstruction can be harnessed to drive reactions. The end point of the process is a reconstructed and thermodynamically stable surface for a fixed polarization: such a surface is not very chemically active and not of interest for catalytic activity to us. To reiterate, we are interested in the transient state of the surface right after polarization change as it begins the process of reconstruction.[33–35]

A previous example of the approach described above has been provided for NO_x direct decomposition on monolayers of CrO_2(RuO_2) on PTO.[34] Below, we discuss this approach in more details beginning with the example of SO_2 oxidation to SO_3. The total overall process comprises a reduction reaction ($O_2(g) \rightarrow 2O(ad)$) and an oxidation reaction ($SO_2(g) + O(ad) \rightarrow SO_3(g)$). By having control over the polarization and hence the surface chemistry, one can drive each half of the process periodically in order to achieve the overall reaction.

3.3. SO_2 oxidation to SO_3 using $PbTiO_3$

Table 2 summarizes the binding energy of SO_2 molecules to the PTO(001) surface. Fig. 2 shows the binding geometries for SO_2 in different polarizations. In positive polarization, SO_2 interacts with the surface strongly. In the paraelectric case, the binding energy is much smaller relative to positive polarization and the binding geometry differs. In negative polarization, SO_3 is formed on the surface because SO_2 takes one of the surface oxygens away. Hence, in negative polarization, it is more informative to describe the configuration as having a SO_3 molecule on a surface with 0.5 ML oxygen vacancies; the computed binding energy is negative (≈ -0.2 eV) meaning the SO_3 desorbs easily. Hence, exposure of the negatively poled stoichiometric PTO to SO_2 molecules causes SO_3 formation and brings the stoichiometric surface to its most stable thermodynamical state which is a surface with 0.5 ML oxygen vacancies.[117]

The current method of producing sulfuric acid is the contact process which was patented in 1831 by Peregrine Phillips.[121,122] At the heart of this process is the rate limiting oxidation of SO_2 to SO_3 in the presence of catalysts such as Pt or V_2O_5. As shown above, negatively poled $PbTiO_3$ has a strong interaction with SO_2 molecules, and, upon adsorption, SO_3 is formed with no barrier and a negligible binding energy. Hence, PTO may be an ideal catalyst for oxidation of SO_2 to SO_3. Namely, after the release of SO_3, we are left with the most thermodynamically stable surface which is a surface with 0.5 ML oxygen vacancies.[35,117] One then changes the polarization to positive or paraelectric state which leads to adsorption of oxygen and replenishment of the vacancies with oxygen atoms. We can thus envisage cyclically converting SO_2 into SO_3.

Table 2 Binding energies of SO_2 in eV on stoichiometric Pb terminated PTO as a function of polarization at 0.5 ML coverage. The binding energy of SO_2 to the negatively poled surface (marked by *) should be interpreted with caution since in this case SO_2 binds to a surface oxygen, forms SO_3 which then desorbs from the surface which now has 0.5 ML O vacancies

Polarization	SO_2 binding (eV)
Positive	1.8
Paraelectric	0.7
Negative	1.2*

We note that the reduction reaction $O_2(g) \rightarrow 2O(ad)$ can proceed by changing the polarization from negative to either a positively polarized or paraelectric phase. While it may seem surprising that an inert surface (paraelectric phase) can be used to run the reduction process, in this context there are oxygen vacancies on the paraelectric surface that have developed through oxidation on the negatively polarized surface ($SO_2(g) + O(ad) \rightarrow SO_3(g)$). In a cyclic scheme, these inherited vacancies render the paraelectric phase reducing upon switching from the negative to the paraelectric state. Fig. 3 shows how 0.5 ML oxygen vacancies dope electrons[209] into the surface conduction bands of the paraelectric state ($\approx$0.5 electron per surface Pb from our calculations). Similar to the positively polarized surface, these doped electrons make the surface oxidizing. Oxygen molecules reduce barrierlessly on such a surface, and the surface achieves its stoichiometric oxygen content.

3.4. NO_x direct decomposition on $PbTiO_3$

NO_x is the generic term for the nitrogen oxides NO and NO_2. They are produced from the reaction between nitrogen and oxygen at high temperatures, *e.g.*, in a car engine. NO_x can react in the atmosphere to form acid rain. Thus environmental regulations are pushing for a sharp decrease in NO_x emission. The main technologies implemented in automotive industries use three-way catalytic converters (TWC) to reduce NO_x to N_2 and O_2[210–217] in which unburnt hydrocarbons and CO are oxidized and NO_x molecules are reduced to N_2 and O_2. The limitation of this method is that, in order to prevent the catalyst from being poisoned (*i.e.*, covered) by oxygen, one needs unburnt hydrocarbons and CO in the gas intake. Hence the engine must operate with a stoichiometric fuel to air ratio whereas an oxygen rich environment (lean burn) would yield a higher energy efficiency and less CO_2 emission.[218–220]

A NO_x direct decomposition catalyst that can operate in a higher oxygen pressure environment has been a long standing goal in the automotive industry.[210,221,222] We show that the switchable out-of-plane polarization of $PbTiO_3$ can effectively control the binding energies of different atoms and molecules that are present in the NO_x direct decomposition process, paving the road for designing an effective catalyst for this reaction and in particular overcoming the problem of oxygen inhibition (poisoning).[223–226]

Below, we investigate the binding of different atomic and molecular species to the PTO surface as a function of ferroelectric polarization. We show that, similar to the cyclic scheme described for NO_x decomposition on CrO_2 or RuO_2 terminated PTO,[34] one can decompose NO_x and form and desorb N_2 in positive polarization while avoiding the oxygen inhibition

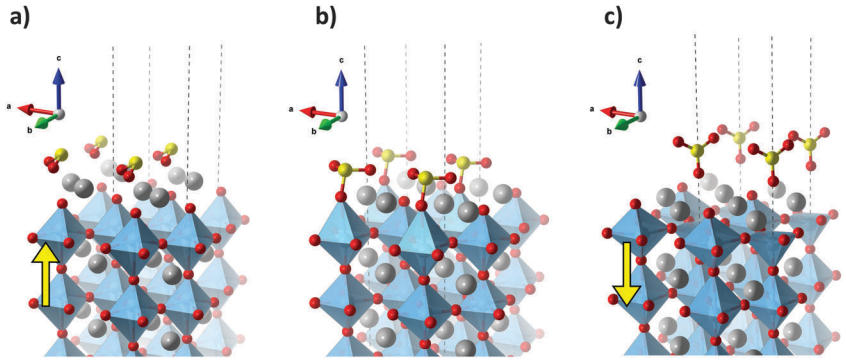

Fig. 2 Binding geometries for SO_2 on the Pb terminated $PbTiO_3$ surface in different polarizations (0.5 ML coverage): (a) positively polarized, (b) paraelectric, and (c) negatively polarized surface. S atoms are shown in yellow, O (red), Pb (gray) and Ti are shown encaged in oxygen octahedra. The yellow arrows show the direction of ferroelectric polarization. On the negatively poled surface, 0.5 ML SO_2 steals 0.5 ML oxygen from the surface octahedra and forms 0.5 ML SO_3 hovering over the surface.

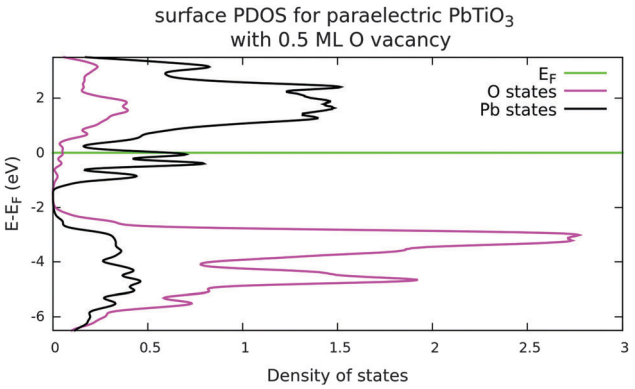

Fig. 3 Projected Density of States (PDOS) on surface Pb and O atoms on paraelectric Pb-terminated $PbTiO_3$ with 0.5 ML O vacancy. The 0.5 ML of oxygen vacancies dope electrons into the surface conduction band dominated by Pb 6p states.

problem by forming and desorbing O_2 in negative or paraelectric phases.

We will be mainly concerned with finding a strategy for NO_x direct decomposition using polarization cycling. However, we have briefly studied the possibility of using positively poled PTO with fixed polarization as a TWC (see ESI†).

3.4.1. NO intact binding. NO binding energies and geometries show significant polarization dependences (see Table 3 and Fig. 4). In negative polarization, NO is bound to a surface oxygen and forms an NO_2 molecule attached to the surface (Fig. 4). For 0.5 ML coverage where half of the surface oxygens bind to NO molecules, the effect of this binding is to drag these surface oxygen atoms by almost 0.9 Å up out of the surface upon forming NO_2. So, it is more sensible to think of this oxygen as part of the NO_2 molecule rather than a part of the surface. We have calculated the binding energy of this NO_2 molecule to the remainder of the surface, which has 0.5 ML O vacancies, to be 0.5 eV per molecule. Since this is much smaller than the 1.9 eV binding energy of NO to the stoichiometric surface, upon heating the surface (for instance in a TPD experiment[71,227,228]), NO_2 will come off the surface (rather than NO) and leave behind a surface with oxygen vacancies. This is

Table 3 NO binding energies and geometries as a function of PTO polarization (the coverage is 0.5 ML NO, *i.e.*, 0.5 NO molecule per 1 × 1 surface unit cell). The binding energy in the negative polarization marked by (*) should be interpreted with caution as we actually have a NO_2 molecule formed which is weakly bound (0.5 eV per molecule) to a surface with 0.5 ML O vacancies

Polarization	Binding geometry	Binding energy (eV)
Positive	NO bridges Pb sites	1.5
Paraelectric	Physisorption	0.3
Negative	NO_2 forms	1.9*

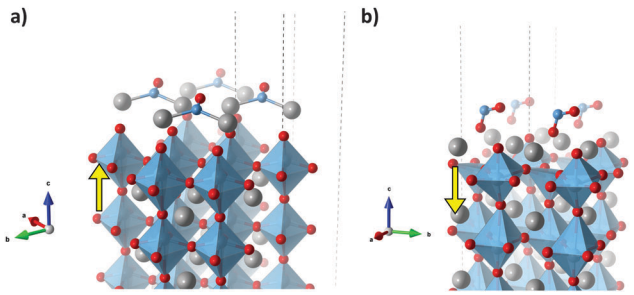

Fig. 4 Comparison of the two binding geometries of NO molecules to PbO terminated PTO (0.5 ML coverage) on (a) positively polarized surface and (b) on negatively poled surface. Nitrogen is shown in pale blue, O (red), Pb (gray) and Ti is encaged in oxygen octahedra. The yellow arrows show the direction of ferroelectric polarization. This figure is rendered using VESTA.[229]

in agreement with prior works showing that the most thermodynamically stable surface for the negatively poled surface is a surface with 0.5 ML oxygen vacancies.[35,117]

In positive polarization, NO bridges between two adjacent Pb atoms (Fig. 4). The attached NO molecule is stretched relative to NO in vacuum, and the interatomic distance is increased by 0.16 Å from 1.17 to 1.33 Å which is the direct consequence of electron transfer from the surface Pb atoms to the attached NO molecule.

In the paraelectric case, the NO molecule simply hovers over the surface with a small binding energy (0.3 eV). In this case, we have a physisorbed molecule on the surface. We note that weak physisorption is expected due to the insulating and inert

nature of paraelectric PTO surface that lacks a density of states at the Fermi energy.

Why are the binding geometries and energies a function of polarization? To answer this question in detail, we study the electronic structure of the surfaces and the NO molecule. We begin by analyzing NO binding to the positively poled PTO. In Fig. 5(a) one can see the Singly Occupied Molecular Orbital (SOMO) and Lowest Unoccupied Molecular Orbital (LUMO) of NO. A SOMO is a molecular orbital that is a half-filled unlike a HOMO that is filled and LUMO that is unfilled. A SOMO acts differently than a HOMO or LUMO in terms of binding. Interaction of the adsorbate's SOMO with both filled (valence) and unfilled (conduction) states of the surface leads to adsorbate stabilization, while the HOMO only has stabilizing interactions with unfilled (conduction) surface states (and the opposite for LUMO). The NO SOMO has π_{2p}* character and spin up while the LUMO has the same character but spin down. Both the NO SOMO and LUMO are localized mainly on the nitrogen atom. This explains our observation that the NO molecule always binds from the N side rather than O side to the PTO surface. The fact that NO binds from the N side to transition metal and oxide surfaces has been discussed.[230–235]

In Fig. 6, one sees the projected density of states (PDOS) on the surface Pb atom before and after 0.5 ML NO adsorption. This explains why NO binding to the Pb atom on the surface of positively poled PTO leads to a considerable stabilization (1.5 eV per molecule): both the NO SOMO and LUMO are below the Fermi level (E_F) of the positively polarized PTO surface by 1.5 eV and 0.2 eV, respectively. In addition to significant electron transfer, there is hybridization with the Pb 6p states (bands) whose center of energy is computed to lie 1.9 eV above E_F. This covalent interaction creates new low energy bonding states on

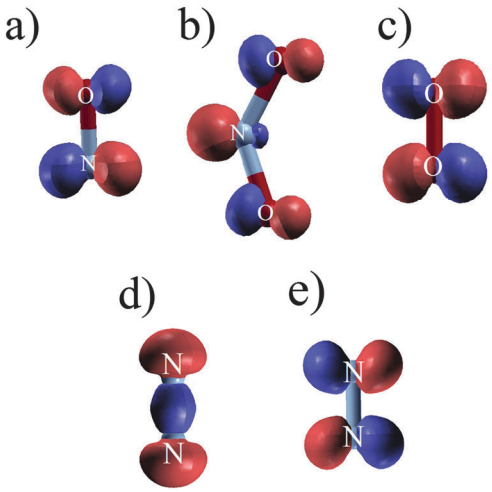

Fig. 5 SOMO, HOMO and LUMO of different molecules. Red shows positive and blue shows negative regions of the wave function. (a) NO: doubly degenerate antibonding state (π_{2p}*), SOMO in spin up and LUMO in spin down channel. (b) NO_2: antibonding state, HOMO in spin up, LUMO in spin down. (c) O_2: doubly degenerate antibonding state (π_{2p}*), HOMO in spin up LUMO in spin down channel. (d) N_2: HOMO (σ_{2p}) (e) N_2: doubly degenerate LUMO (π_{2p}*).

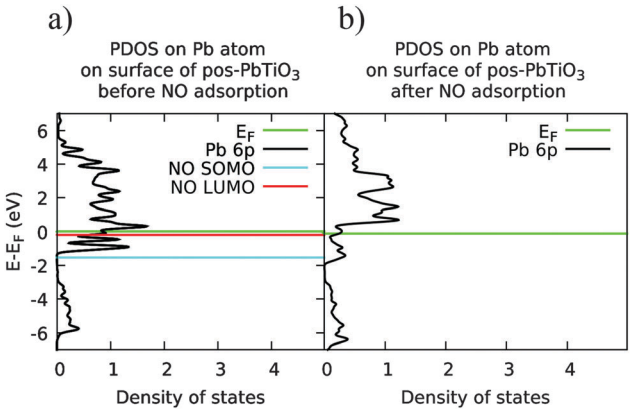

Fig. 6 PDOS on surface Pb atom in positively poled PTO (a) before, (b) after adsorption of 0.5 ML NO. For simplicity only the Pb 6p states are shown (they dominate the surface conduction band).

the surface which have mostly NO π_{2p}* character and lie below E_F; it also leads to the creation of antibonding states which have mostly Pb 6p character and lie above E_F. Consequently, the center of Pb 6p band is expected to be pushed up in energy. Fig. 6(b) shows the PDOS on a Pb surface atom after NO adsorption at 0.5 ML coverage: the center of Pb 6p band is confirmed to be pushed up by 0.9 eV. The fact that the center of the Pb 6p band has moved up in energy decreases the interaction of this band with subsequent NO molecules that attach to this surface. In addition, the decreased density of states below the Fermi energy leads to lower subsequent electron transfer. Both of these trends should lead to a reduced binding energy per molecule at higher NO coverages. We have confirmed this prediction by computing the NO binding energy for 1 ML coverage which is 0.9 eV per NO molecule (0.6 eV lower than its value in 0.5 ML coverage). This adsorbate self poisoning effect has been explained in the literature through consideration of surface band mediated interactions and the density of states near the Fermi energy.[236–239]

We have also computed the real space electron density transfer upon adsorption of 0.5 ML NO molecules which is shown in Fig. 7. It can be seen that electrons populate the NO π_{2p}* states; electrons are depopulated from regions close to surface Pb atoms that are adjacent to the N end of the NO molecule and from the Pb dimers (Pb atoms 3.24 Å apart from each other) that are

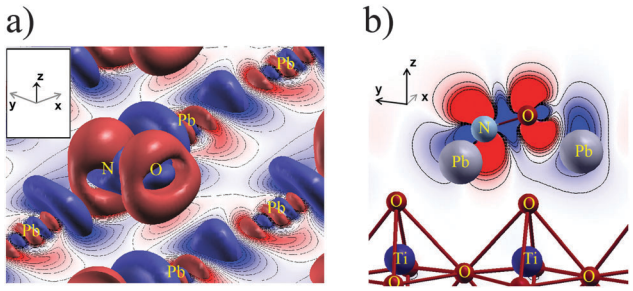

Fig. 7 Electron density transfer in real space due to adsorption of 0.5 ML NO on positively poled PTO: (a) top (b) side view. Blue shows electron loss, red electron gain. This figure has been rendered using structure visualization program XCrySDen.[241]

adjacent to the O end of the NO. This electron transfer to the NO molecule also shows up in the Lowdin charge[240] on the NO molecule before and after adsorption to the positively polarized PTO surface: it increases by almost 0.8 *e* per molecule. The increase in NO interatomic distance (stretching) by 0.16 Å upon binding is a result of this transfer of about 0.8 electron to the antibonding NO π_{2p}* states.

Now we turn our attention to the negatively polarized surface. Fig. 8 shows the PDOS on the surface oxygen before and after NO adsorption. In Fig. 8(a) one notices that the SOMO of NO is slightly below the E_F of the clean negatively poled surface by 0.2 eV; this should be compared with the case of the NO molecule on the positively poled surface (Fig. 6) where the SOMO is 1.5 eV below E_F. Hence, unlike the positive polarization case, one would not expect a sizable electron transfer to the NO molecule but would predict hybridization between the NO SOMO and the center of O 2p band which lies 1 eV below it and is partially filled. This hybridization would push down the partially occupied surface O 2p bands to lower energies, enhance their bonding character and increase stability.

Based on these arguments, one predicts a large binding energy between the NO molecule and the stoichiometric negatively poled PTO surface which is confirmed in Table 3. At 0.5 ML NO coverage, there are two types of surface oxygen atoms (see Fig. 4(a)): the first type has an NO molecule attached to it, while the second type has no molecules attached to it. By looking at the PDOS on the second type of oxygen (Fig. 8(b)) we can learn about the coverage dependence for negative polarization. Here, the O 2p bands have less density of states at E_F after NO adsorption compared to before adsorption. We count the number of holes in the O 2p bands by integrating the portion of those bands above E_F and find that that adsorption of 0.5 ML NO molecule decreases the number of holes on this oxygen atom from 0.48 to 0.19. This decrease might lead us to expect that, similar to the case of NO adsorption on positively poled PTO, the binding energy of NO for a higher coverage (1 ML) should decrease following the reasoning of Feibelman *et al.* (based on the density of states at Fermi energy).[236] However, unlike the positive polarization case, here the bonding is mostly covalent as opposed to charge transfer. Thus it is the center of the O 2p band that dictates the coverage dependence and not the density of states at E_F. We have calculated the center of the O 2p band (on the first type of oxygen) to be 1.2 eV below E_F after NO adsorption which is the same as before adsorption. This justifies our observation that the NO binding energy is unchanged at 1.9 eV per NO when going from 0.5 to 1.0 ML coverage.

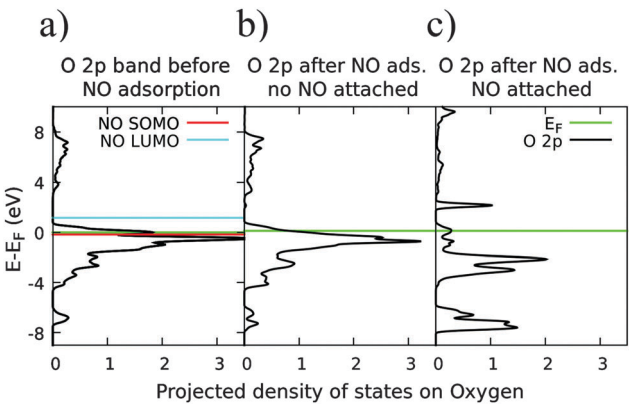

Fig. 8 Negatively polarized PTO: projected density of states (PDOS) (on a negatively polarized PTO sample) on (a) a surface oxygen before NO adsorption, (b) a surface oxygen which does not directly bond to an NO, and (c) a surface oxygen directly attached to an NO molecule. For simplicity only the O 2p states are shown (they dominate the surface valence band).

Now we turn our attention to the first type of oxygen atoms which bind directly to NO molecules. As Fig. 8(c) shows, the O 2p projection on these atoms experiences striking changes due to the bonding. There are many new features that did not exist prior to the adsorption of the NO molecule. As mentioned above, this binding process leads to formation of 0.5 ML NO_2 physisorbed on the rest of the surface so that this oxygen has experienced strong perturbations.

3.4.2. O_2 binding. We now describe intact and dissociative binding of O_2 in each polarization state. Oxygen binding energies depend strongly on the polarization (Table 4). In positive polarization, the ground state of binding is dissociative and exothermic by 2.6 eV per molecule (at 0.5 ML coverage). We have tried several initial geometries for our relaxations, and the only metastable state that we found resembling an intact binding mode was a "pseudo-intact" and stretched O_2 molecule in which the O atoms have an interatomic distance of 1.57 Å compared to 1.24 Å for gas phase O_2. The dissociative mode in positive polarization consists of separated O atoms located between Pb atoms as can be seen in Fig. 9(a).

In the paraelectric phase, unlike positive polarization, the ground state is a weak physisorption. The dissociative binding mode in this case has almost the same geometry as in the positive case, but very different energetics (see Table 4) due to the lack of electron doping of the surface.

In negative polarization, the intact binding mode is a physisorbed molecule with negligible binding energy. The dissociative binding geometry is different from the positive and paraelectric case as can be seen in Fig. 9(b): now each oxygen adsorbate binds to a surface oxygen atom. This can be thought of as an oxygen atom forming an O_2 molecule with one of the surface oxygens after dissociation. The dissociative binding energy is very small in this case. Table 4 shows how changing the polarization of PTO can strongly modify the behavior of its surface towards oxygen. The positively polarized surface is very strongly interacting with

Table 4 Intact and dissociative binding energies for an O_2 molecule on the PTO surface as a function of polarization relative to O_2 in vacuum. More positive a numbers mean the binding is more favorable. A negative number indicates a metastable state which is less favorable than O_2 in vacuum

Polarization	Intact binding energy (eV)	Dissociative binding energy (eV)
Positive	2.4	2.6
Paraelectric	0.2	−0.8
Negative	0	0.4

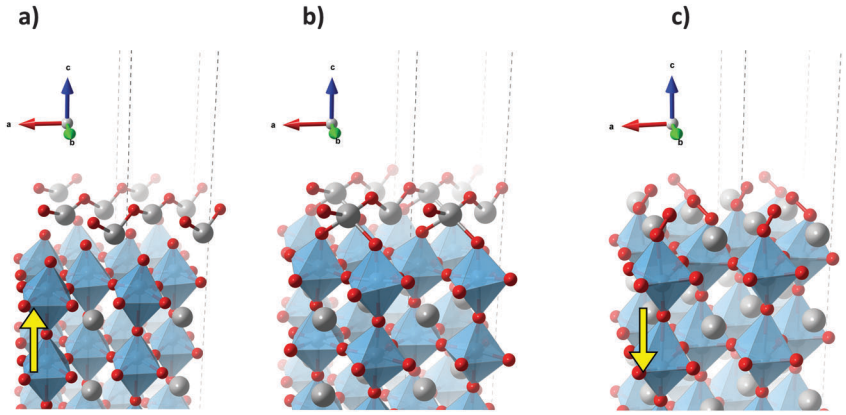

Fig. 9 The binding geometry for dissociated binding of O_2 to PTO surface on (a) positively polarized surface, (b) paraelectric and (c) negatively polarized surface. Oxygen is shown in red, Pb (gray) and Ti is encaged in oxygen octahedra. The yellow arrows show the direction of ferroelectric polarization.

O_2 while negatively polarized and paraelectric polarizations are weakly interacting.

For catalytic applications, this is a very promising finding since one of the main challenges in NO_x direct decomposition using conventional catalysis methods is that if the surface–NO_x interaction is strong enough to dissociate the NO_x molecules then it is very difficult to desorb resulting oxygen atoms: they gradually poison the catalyst[224,242] by blocking the catalytic sites. This problem is referred to as oxygen inhibition.[223,225,226,243–246] As shown here, we can avoid this problem by actively toggling the surface–adsorbate interaction by using ferroelectric polarization as a switch.

Fig. 10 shows the level alignment of the surface Pb states of positively poled PTO with the O_2 HOMO and LUMO. The oxygen's LUMO lies 0.6 eV below the E_F of the surface so there is electron transfer to the O_2 LUMO. Since the O_2 LUMO is an antibonding state (π_{2p}^*), the O–O bond loosens: we find that the elongation is sufficient to make the molecule barrierlessly dissociate into O atoms. Fig. 11 shows the metastable "pseudo-intact" state in which the O_2 molecule is in between two Pb atoms and is highly stretched. We can see that electrons are transferred to the O_2 LUMO from surface Pb atoms. This electron transfer to an antibonding molecular state justifies the computed increase in the bond length of O_2 and quenching of magnetic moment from 2 μ_B to 0.3 μ_B per molecule.

The reason behind the difference in oxygen binding energies in different polarizations is the difference in position of conduction and valence band edges of the surface relative to the O_2 HOMO and LUMO. As Fig. 12 shows, unlike the positively polarized case, binding of the O_2 molecule to the paraelectric surface should not be strong since the HOMO energy is already below E_F and the LUMO energy is in the insulating surface energy gap. Of course, there are, in principle, two covalent interactions that could lead to some stabilization: (1) interaction of the empty O_2 LUMO with the center of the filled surface O 2p bands (which are 4.8 eV apart), and (2) interaction of the center of empty surface Pb 6p band with the O_2 HOMO (which are 4.6 eV apart). In practice, both are far separated in energy and lead to very weak binding.

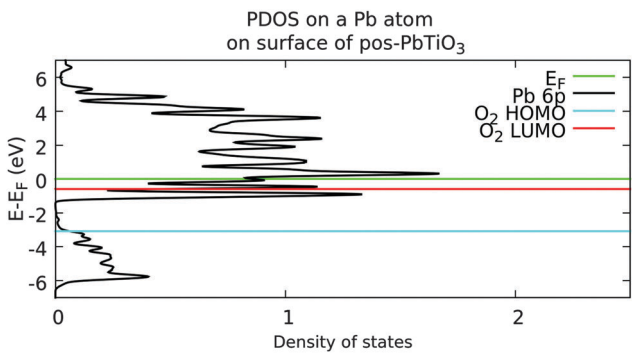

Fig. 10 Projected density of states (PDOS) on a Pb atom on the positive PTO surface and its relative alignment with O_2 HOMO and LUMO. For simplicity only the Pb 6p states are shown (they dominate the surface conduction band).

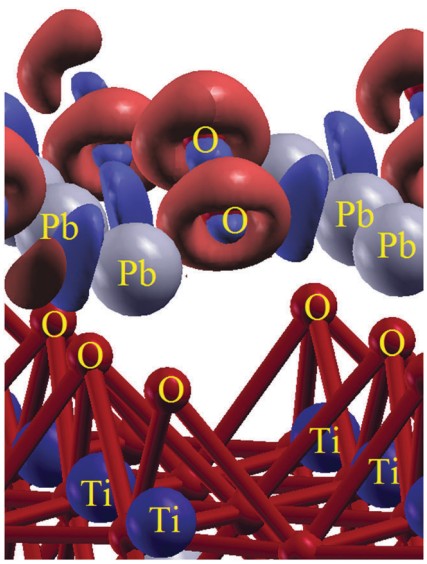

Fig. 11 Real space electron transfer from Pb states to the O_2 LUMO for the "pseudo-intact" structure on positively poled Pb terminated PTO. Red shows gain of electrons, and blue shows loss of electrons.

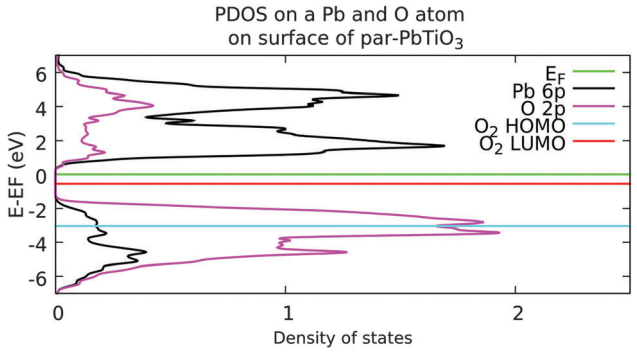

Fig. 12 Projected density of states (PDOS) on the surface Pb and O atom on the paraelectric PTO surface and their relative alignment with O_2 HOMO and LUMO.

3.4.3. N_2 binding. For all polarizations, the binding energy of N_2 molecules is found to be small to the surfaces (0.1 eV for both positive and paraelectric polarizations, and 0.5 eV for negative). The dissociative binding modes are completely unstable as the separated N atoms always recombine with each other (with no energy barrier) to form N_2 molecules. The fact that N_2 in both intact and dissociative binding modes has negligible interaction with the PTO surfaces is good news for NO_x direct decomposition: N_2 molecules can easily form from separated N atoms, which are the results of NO dissociation, and leave the surface.

3.4.4. N and O atomic binding. Fig. 13 shows the binding geometries of O atoms to the PTO surface in different polarizations. One can see that on positively polarized PTO, oxygen bridges between two Pb atoms (the top Pb atoms have experienced "sliding" as mentioned above). On the paraelectric surface, oxygen binds to one of the surface oxygens in addition to two adjacent Pb atoms. Atomic binding energies for O on PTO can be found in Table 5 relative to two different references: an O_2 molecule in vacuum and an O atom in vacuum. One can see that in positive polarization, O atoms bind favorably to the surface, while on the paraelectric surface there is only a metastable state that is 0.7 eV per atom less favorable than O_2 in vacuum. On the negatively poled surface, no metastable atomic oxygen binding mode was found: we tried many different initial geometries for our relaxations but

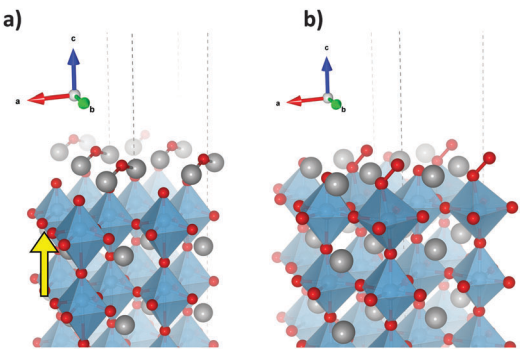

Fig. 13 Binding of atomic oxygen to (a) positively poled, (b) paraelectric PTO surfaces (0.5 ML coverage). Oxygen is shown in red, Pb (gray) and Ti are encaged in oxygen octahedra. In (a), the yellow arrow shows the direction of ferroelectric polarization.

Table 5 Binding energies (eV) for atomic adsorption of an O atom on Pb-terminated PTO as a function of polarization (0.5 ML coverage). NS means no mechanically stable configuration exists

Polarization	Binding energy relative to O_2 in vacuum (eV)	Binding energy relative to O in vacuum (eV)
Positive	3.0	6.3
Paraelectric	−0.7	2.6
Negative	NS	NS

all led to a barrierless process where a surface O atom joined with the adsorbed O atom to form O_2 reflecting the fact that the negatively poled surface is extremely oxidizing. The binding energy of this formed O_2 molecule to the remainder of the surface, which now has an oxygen vacancy, is −0.1 eV (*i.e.*, unstable) relative to O_2 in vacuum so it readily leaves the surface. Again, these findings agree with the fact that the most stable surface structure for negative polarization has 0.5 ML O vacancies.[35,117]

Now we look at the atomic binding of N to the PTO surface in different polarizations. The binding geometries are very similar to the case of oxygen atomic binding. In negative polarization, atomic binding of nitrogen to the surface is so unfavorable that we do not find a metastable binding mode: the N atom steals one of the surface oxygens and forms NO. The binding energy of this formed NO molecule to the surface with 0.5 ML oxygen vacancies is 0.3 eV relative to NO in vacuum, so it easily leaves the surface. As per Table 6, polarization affects the binding energy of N to the surface by more than 2 eV per atom.

We have calculated the coverage dependences for both N and O atomic bindings to the positively poled surface. The results are summarized in Table 7 which shows two different trends. For N, changing the coverage from 0.25 ML to 1 ML decreases the binding energy per atom by 1 eV every time we double the coverage. But for O, going from 0.25 ML coverage to 0.5 ML increases the binding energy slightly by 0.2 eV per atom while increasing the coverage further to 1 ML decreases the binding energy by 1.7 eV.

We rationalize these trends based on electron counting. Oxygen and nitrogen are both very electronegative atoms:[247,248] they can accordingly accommodate 2 and 3 electrons respectively to become closed shell. The magnitude $|\vec{P}|$ of the bulk polarization of $PbTiO_3$ corresponds to $\approx$1 fundamental unit of charge per primitive 1 × 1 surface unit cell (s.u.c.)[34,35,200,201] which is also the magnitude of the surface doping (compensating) charge. At 0.25 ML coverage in positive polarization, we have close to 4 doped electrons per adsorbate. This many electrons can stabilize either N or O, thus we expect large binding energies

Table 6 Binding energies (eV) for atomic adsorption mode of N on Pb-terminated PTO as a function of polarization (0.5 ML coverage). NS means no mechanically stable configuration exists

Polarization	Binding energy relative to N_2 in vacuum (eV)	Binding energy relative to N in vacuum (eV)
Positive	−1.6	3.3
Paraelectric	−3.6	1.3
Negative	NS	NS

Table 7 Coverage dependences for N and O atomic binding energies (relative to an atom in vacuum) for positively polarized PTO surface

Coverage	N binding energy (eV) relative to N in vacuum	O binding energy (eV) relative to O in vacuum
0.25 ML	4.3	6.1
0.5 ML	3.3	6.3
1 ML	2.3	4.6

for both species at this coverage. In 0.5 ML coverage, we have about 2 extra electrons per adsorbate: this is enough to completely stabilize oxygen and make it closed shell, but it is not enough to completely stabilize nitrogen. This is why the binding energy per atom is essentially unchanged for O but decreases for N. In 1 ML coverage, we have almost 1 extra electron per adsorbate so even oxygen cannot reach a closed shell configuration. That is why in going from 0.5 to 1 ML coverage the oxygen binding energy per atom drops significantly. In the case of transition metal surfaces, there are several studies to support this electron transfer picture which shows itself as an induced dipole moment on the surface and an increased work function:[249,250] the induced dipole moment decreases with coverage as does the electron transfer to the adsorbates.[251–253] Below, this simple electron transfer picture will be confirmed by examining the surface and adsorbate electronic structure.

The problem of coverage dependence (self-poisoning) of nitrogen, oxygen, sulfur and carbon adsorbates is discussed in the literature mostly for transition metal surfaces and not for perovskite or ferroelectric surfaces. For example,[254] the coverage dependence of oxygen, nitrogen, and carbon atomic binding energies to the Pd(111) surface was addressed based on a simple d-band model.[255–258] The coverage dependence for N and O atomic binding energies spanned a 1.5 eV range from low (0.2 ML) to full coverage (1 ML), and the dependence of adsorption energies on coverage varied systematically from C to O and in a linear fashion for each, carbon being the most sensitive and oxygen the least. Here, we see a coverage dependence for adsorption energies that spans even a larger range of 2 eV. Unlike nitrogen atoms on PTO, and unlike the trends seen in literature for S, C, O and N on various transition metal surfaces,[251–254,259–264] the coverage dependence for oxygen in our case is not linear in the 0.25 to 1 ML range.

Fig. 14 shows the electron density transfer in real space upon adsorption of 0.25 ML N to the positively poled PTO surface: the electrons leave the Pb atoms and migrate to the N unoccupied 2p atomic states. The spherical symmetry of the electron transfer to the N atom indicates that it has reached a closed shell configuration by accepting 3 electrons.

Fig. 15 confirms our electron transfer picture. At low coverage (0.25 ML), all adsorbate 2p states remain very atomic-like with sharp peaks in the densities of states. The N 2p states are higher in energy than those of the more electronegative O 2p. Fig. 15 also shows that the O 2p states are below E_F in both 0.25 and 0.5 ML coverage which means oxygen reaches a closed shell configuration in both cases. The sharp nature of the O 2p states and their small hybridization with the surface Pb 6p states show that the

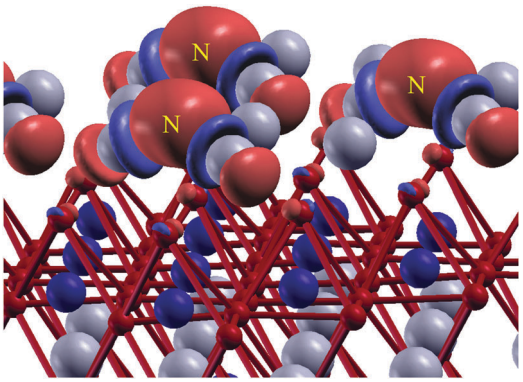

Fig. 14 Electron density transfer in real space upon adsorption of 0.25 ML nitrogen to the positively poled PTO surface. N atoms bridge in between Pb atoms. Red indicates the region of space which electrons migrate to, while the blue indicates the region which electrons migrate from upon adsorption of 0.25 ML nitrogen atoms.

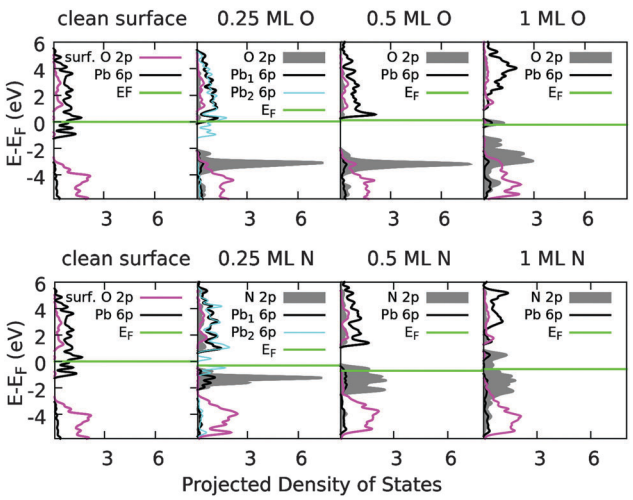

Fig. 15 Projected density of states (PDOS) for binding of N and O atoms to the positively poled stoichiometric surface. The "clean surface" panels show the PDOS for surface Pb atoms (which dominates the surface conduction band) and surface oxygens (which dominates the surface valence band). The other panels show PDOS for adsorbed O and N for 3 different coverages. For the panels for 0.25 ML coverage, the surface has two different kinds of Pb: Pb_1 binds to the adsorbate while Pb_2 does not.

nature of O binding to the surface is primarily due to electron transfer and not covalency. In 1 ML coverage, the O 2p state is no longer fully occupied and it experiences more dispersion due to oxygen–oxygen interactions.

As Fig. 15 shows, for 0.25 ML coverage, the sharp atomic-like N 2p states are below the Fermi energy. In addition, at 0.25 ML coverage, there is more hybridization between Pb 6p and N 2p states compared to O 2p at the same coverage. This is due to the fact that N 2p states are higher in energy and closer in energy to both the Fermi energy and the center of the Pb 6p band. As discussed above, in 0.5 ML N coverage the surface doesn't have enough electrons to fully populate the empty N 2p states: this is confirmed in Fig. 15 in which some of the N 2p states are now depopulated and above the Fermi level. This is also the case for

Table 8 Binding energies (in eV and relative to NO in vacuum) for the NO molecule in both dissociated and intact binding mode for two different NO coverages on positively polarized PTO. In 0.5 ML coverage, the intact mode is more favorable while in 0.25 ML the opposite is true

	Coverage	
Binding mode	0.25 ML	0.5 ML
Dissociated	2.4	−0.4
Intact	1.9	1.5

1 ML N coverage. One should note that due to the larger hybridization between N 2p and Pb 6p states compared to the case of oxygen, there is a stronger surface band mediated interaction among the N adsorbates relative to O adsorbates. This can be best seen at 0.5 ML coverage where we still have atomic-like O 2p states while the N 2p band has a noticeable dispersion due to surface-band-mediated interaction with other nitrogen adsorbates.

3.4.5. NO dissociative binding. Having investigated N and O atomic binding to the positively polarized PTO surface, we turn our attention to NO dissociated binding on this surface. As can be seen in Table 8, at 0.25 ML NO coverage (as opposed to 0.5 ML coverage), the dissociated binding mode is more favorable than intact molecular binding.

This coverage dependence can be understood based on the electron transfer picture explained in the previous section. At 0.5 ML NO coverage, the surface has only 2 extra electrons to offer to the atomic adsorbates (1 N and 1 O). This number of electrons can make the more electronegative O reach a closed-shell configuration, but then there is no electron left to stabilize the N binding: this explains why NO dissociated binding is not stable in this case (see Table 8). At 0.25 ML NO coverage, there are 4 electrons for 2 adsorbates (1 N and 1 O): the more electronegative O becomes closed shell while 2 electrons are left for N to stabilize its binding to the surface. Based on this reasoning, we predict that the dissociated binding energy will be maximized near 0.2 ML NO coverage and should stay constant for smaller coverages.

The fact that the ground state of bound NO on the surface is its dissociated state means one can dissociate NO molecules using the positively polarized PTO surface at low coverage. The process we propose is the following. First, the NO will bind and dissociate: our calculated NO dissociation barrier, using the constrained relaxation method,[194,195] is 0.7 eV. Next, at 0.25 ML NO coverage, it is more favorable for separated N atoms to form N_2 molecules, and the calculated N diffusion barrier on positively poled PTO is calculated to be $\approx$1 eV which is a reasonably small value (it is lower than the calculated O diffusion barrier by 0.1 eV). The weakly bound N_2 molecules then leave the surface behind and 0.25 ML O adatoms remain attached. This N_2 desorption reaction on positively poled surface is exothermic by 2.7 eV per N_2 molecule.

Thus one should be able to dissociate NO and form N_2 for low NO coverages ($\leq$0.25 ML), but once the surface begins to be saturated with oxygen atoms (either from NO dissociation or O_2 dissociation), NO decomposition will halt. Then one can

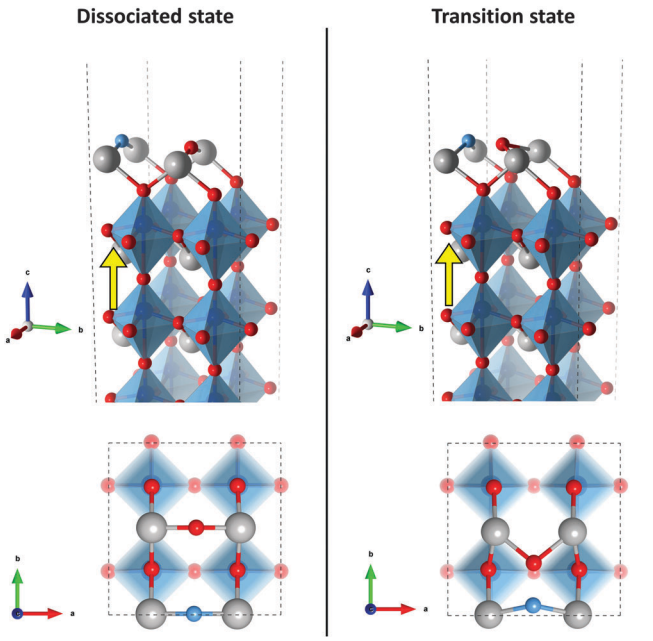

Fig. 16 Comparison of the transition state (TS) and dissociated binding mode for NO on positively poled PTO at 0.25 ML coverage. A side view of the surface is shown on top while a top view is shown on the bottom. The color code is N (pale blue), O (red), Pb (gray), and Ti are encaged in blue oxygen octahedra. The yellow arrows show the direction of ferroelectric polarization. At the TS, the N–O distance is 1.89 Å while at the dissociated state it is 3.86 Å. The Pb–O distances are 2.26 and 2.06 Å in the TS and dissociated state, respectively. The Pb–N distance is 2.18 and 2.06 Å in the TS and dissociated state, respectively.

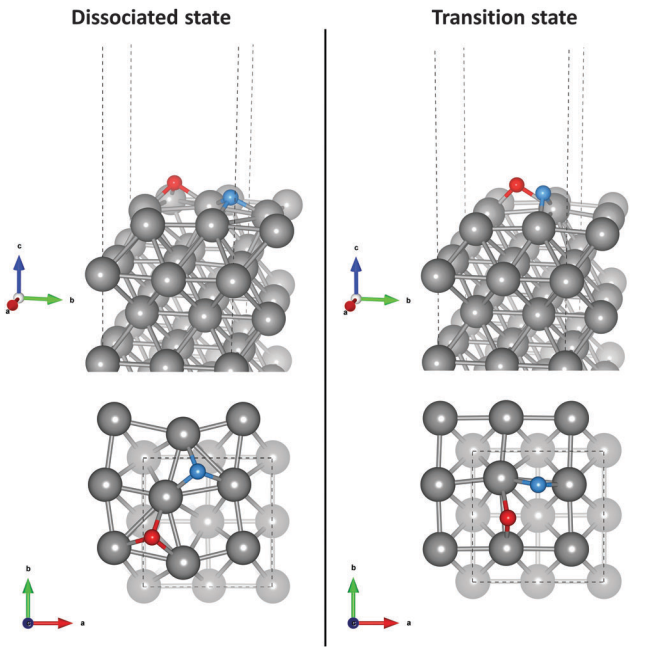

Fig. 17 Comparison of the transition state and the dissociated binding mode for NO on Pt(001) transition metal surface. Side view of the surface is shown on top while a top view is shown at the bottom. The color code is N (pale blue), O (red) and Pt (gray). At transition state the N–O distance is $\approx$1.95 Å while at the dissociated state it is $\approx$3.55 Å. The Pt–O distance is 2.04 and 2.08 Å in the TS and dissociated state, respectively. The Pt–N distance is 1.93 and 1.96 Å in the TS and dissociated state, respectively.

switch[265–275] the polarization to negative (using an electric field) or to paraelectric (using a temperature increase): in both phases the oxygen binding to the surface is weak and one can clean off the oxygens from the surface, bringing back the surface to the pristine state and ready for the next polarization cycle.

Fig. 16 depicts the transition state for NO dissociation on positively poled PTO at 0.25 ML coverage. The N–O distance is ≈1.9 Å and resembles a highly stretched molecule. This is similar to the case of the dissociation of diatomic molecules on transition metal surfaces (*e.g.*, see Fig. 17) where one of the adsorbate atoms is already close to its final dissociated position while the other is on its way.[276–278] In the case of transition metals,[276] for such "stretched" transition states, the electronic structure of the transition state (TS) is more like that of the adsorbed atoms than that of the adsorbed molecule, as verified by our example calculation (see Fig. 18). However, in the case of NO dissociation on ferroelectric $PbTiO_3$, Fig. 19 shows that such a resemblance is not observed in the density of states.

One major difference is that in the case of transition metals, as exemplified by NO binding to Pt(001), there is a significant hybridization between the adsorbate and metal electronic states for both the TS and dissociated configurations. In contrast, on positively polarized PTO, hybridization between the adsorbate and the surface for the dissociated configuration is very weak unlike the TS configuration. We believe that a major reason for the difference between the positively poled oxide and transition metal surface is that the oxide surface has a considerable energy band gap (≈1.7 eV in our DFT calculations) and the adsorbate states either align with the edge of the valence band (oxygen adsorbates) or the middle of the band gap (nitrogen adsorbates) (see Fig. 15). In both cases, the adsorbates do not have states close to the Fermi level. Thus, in order to create a significant covalent bond between the adsorbate and the surface, the surface must deform mechanically to make the energy of the surface states approach those of the adsorbates and this deformation costs energy. The positively poled surface has a reservoir of high energy doped electrons near the edge of the conduction band which can transfer to the low-energy atomic-like adsorbate states and stabilize their binding with the surface (see Fig. 20): this is binding *via* charge transfer and not covalency, so the surface does not need to deform mechanically. The simultaneous existence of a parallel channel for binding (charge transfer in

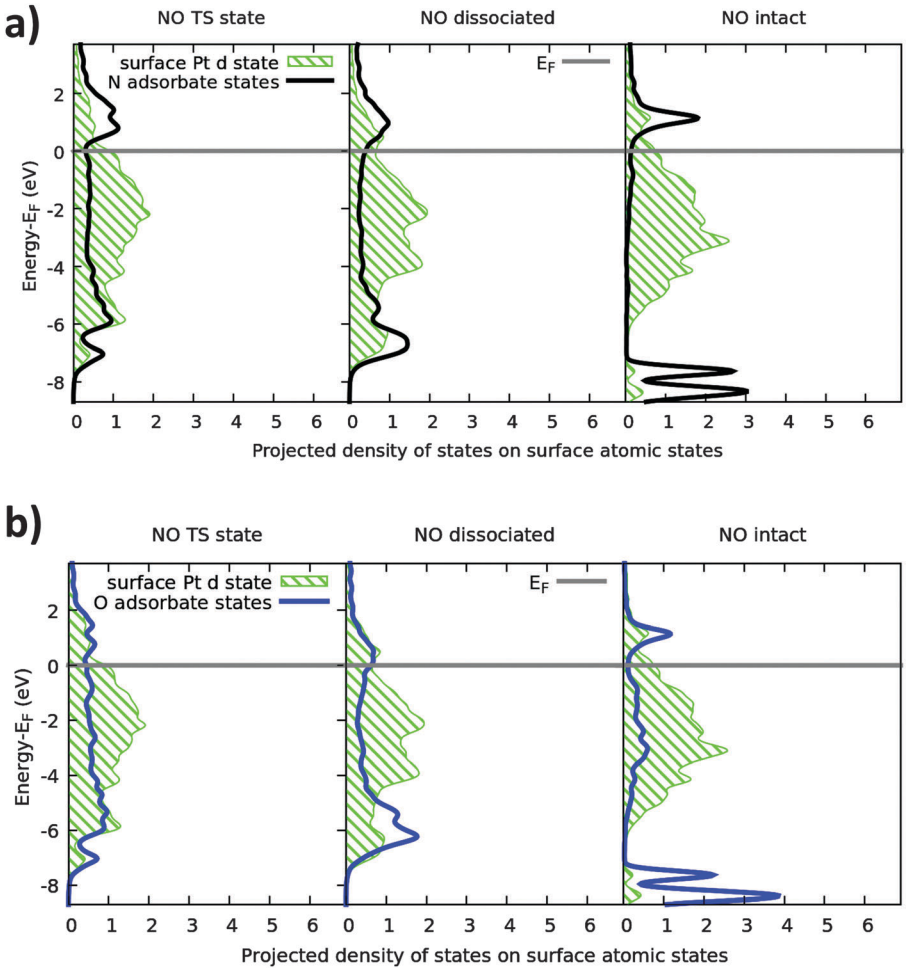

Fig. 18 Comparison of the electronic structure of the transition state (TS), dissociated and intact binding state for NO on the transition metal surface Pt(001). (a) Projected density of states (PDOS) of the adsorbed nitrogen and surface Pt. (b) PDOS of adsorbed oxygen and surface Pt. The electronic structure of the transition state resembles the electronic structure of the dissociated rather than the intact binding configuration.

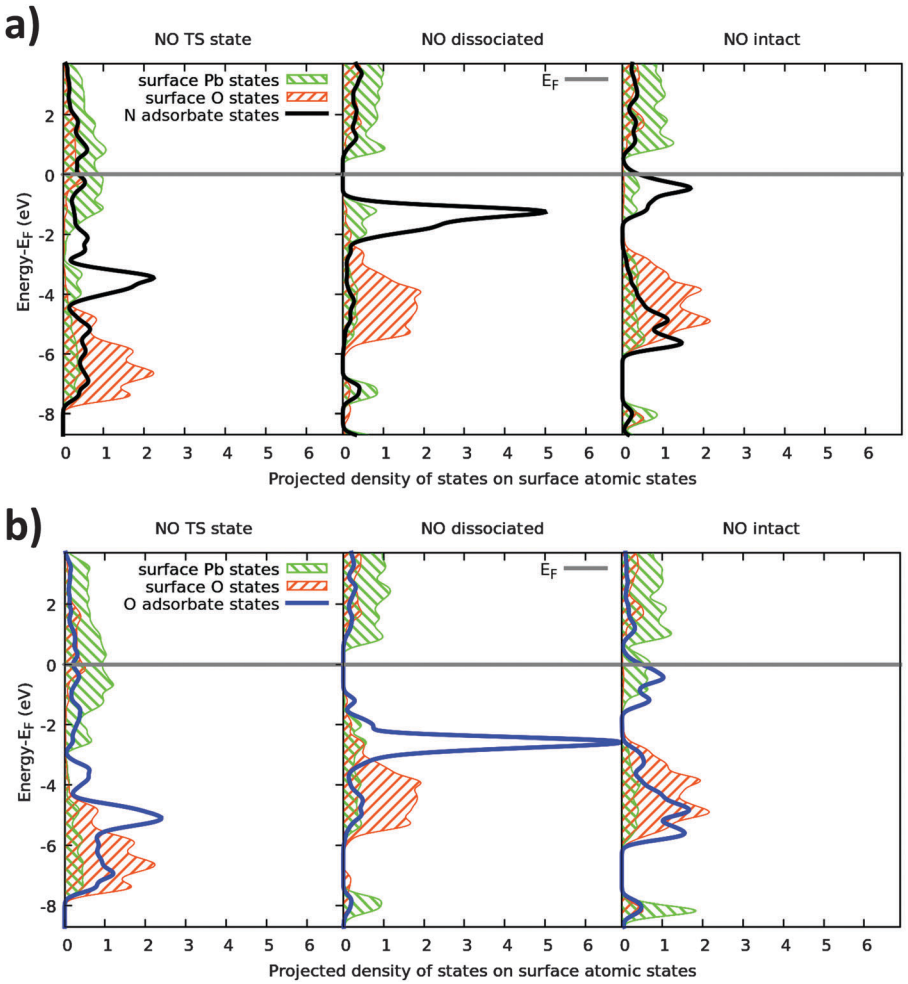

Fig. 19 Comparison of the electronic structure of the transition (TS), dissociated and intact binding states for NO on positively poled $PbTiO_3$(001) at 0.25 ML NO coverage. (a) Projected density of states (PDOS) on adsorbed nitrogen. (b) PDOS on adsorbed oxygen. Unlike the case of dissociation on transition metals, the electronic structure of the transition state does not resemble the electronic structure of the dissociated state.

addition to covalent surface–adsorbate interactions) and an energy gap near the Fermi energy is likely the basic cause of the difference. This observation may open an avenue for breaking the scaling relations between the TS and dissociated binding energies which have been identified as a limiting factor in designing efficient and selective catalysts.[8,9,33] The existence of extra doped mobile charges on the surface of a gapped oxide might play the role of an extra degree of freedom[29] sought in the transition metal literature and which has been deemed necessary to break away from the scaling relations.

3.4.6. NO_2 intact and dissociative binding. As explained above, NO can be dissociated into N_2 and O_2 at low coverages ($\leq$0.25 ML). Here we show that one can use the positive polarization to decompose NO_2 into NO and O even at higher coverages (0.5 ML). The resulting NO can later be dissociated into N and O in the same polarization state as described above. Table 9 summarizes the NO_2 binding energies and geometries for different polarizations: NO_2 interacts strongly with the positively poled PTO surface. Fig. 21 depicts the intact binding of NO_2 to the positive PTO surface. The mechanism behind this binding is a significant electron transfer from the Pb-dominated conduction bands to the NO_2 antibonding LUMO which results in a weakening and elongation of the N–O bond (by 0.13 Å relative to NO_2 in vacuum). The NO_2 dissociation barrier calculated using the constrained relaxation method is found to be very small ($<$0.1 eV). As Table 9 shows, for positive polarization the ground state for bound NO_2 has it dissociated into O and NO.

3.4.7. NO_x direct decomposition on $PbTiO_3$ summary. In brief, NO and NO_2 both prefer to dissociate to form bound N and O on the positively poled PTO surface at reasonably low coverages ($\leq$0.25 ML). Two such N atoms prefer to pair up and form N_2 which is weakly bound and leaves the surface. The surface is then poisoned with strongly bound O atoms. One can then clean the poisoned surface by changing polarization to either negative or paraelectric, and the oxygen is weakly bound and leaves. Once clean, the surface can be brought back to positive polarization, ready for the next cycle. One uses positive polarization for the reduction half of the reaction (NO/NO_2 reduction) and negative/paraelectric for the oxidation part ($O + O \rightarrow O_2$) thereby completing the overall $2NO \rightarrow N_2 + O_2$ or $2NO_2 \rightarrow N_2 + 2O_2$ decomposition reactions.

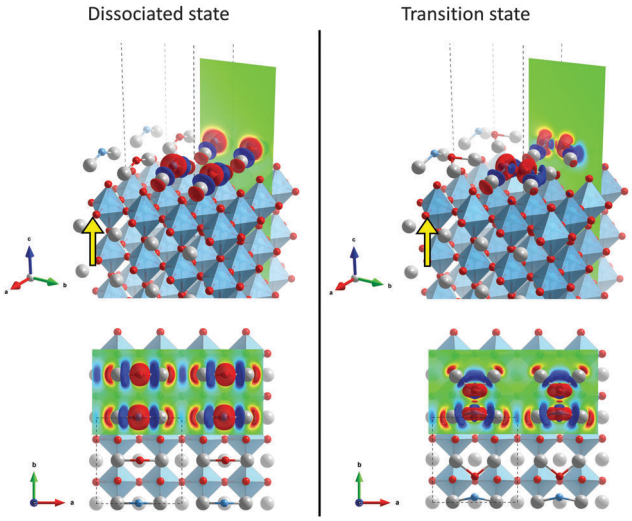

Fig. 20 Comparison of NO binding to positively poled $PbTiO_3$ (at 0.25 ML NO coverage), in transition and dissociated state using real space electron redistribution. Nitrogen is shown in pale blue, O (red), Pb (gray) and Ti is encaged in oxygen octahedra. The yellow arrows show the direction of ferroelectric polarization. Top panels show the side view, while the bottom panels show the top view of the surface. The color red shows the regions of space which electrons migrate to, while the blue regions indicate electron depopulation. As it can be seen, in the dissociated state, as opposed to the TS, there is not a significant hybridization between the adsorbate and surface states, and the charge transfer is between the surface and a spherically symmetric distribution on the adsorbates. A color scale has been used for 2-d electron redistribution sections in which red shows positive (population by electrons), blue indicates negative (depopulation by electrons) and green is neutral.

Table 9 NO_2 binding energies and geometries on Pb-term PTO as a function of polarization

Polarization	Binding energy (eV)	Binding geometry
Positive	1.9	Intact: NO_2 bridges between two leads
Positive	2.3	Dissociated: O bridges between two Pb NO is physisorbed
Paraelectric	0.5	Intact: physisorption
Negative	1.5	Dissociated: forms nitrate with surface O atom

3.5. Direct partial oxidation of methane to methanol

We now investigate whether the cycle described above for SO_2 oxidation into SO_3 can be used to achieve direct partial oxidation of methane (CH_4) to methanol (CH_3OH). In such a cycle, methane can react with the oxidizing (negatively poled) surface to produce methanol. Then, one switches the polarization to the reducing state (positive polarization where oxygen molecules dissociate with zero barrier in our calculations) and replenishes the missing oxygens, making the surface ready to become oxidizing again upon polarization switching. The overall effect of such a cycle will be the direct partial oxidation of methane to methanol, $CH_4(g) + 1/2O_2(g) \rightarrow CH_3OH(g)$.

One can envisage an oxidizing/reducing cycle on either (a) bare ferroelectrics, or (b) transition metal oxide terminated ferroelectrics as exemplified in other work.[35] The simpler approach is to use a bare ferroelectric surface. Below, we examine the possibility of using bare PTO to catalyze the partial oxidation of methane to methanol.

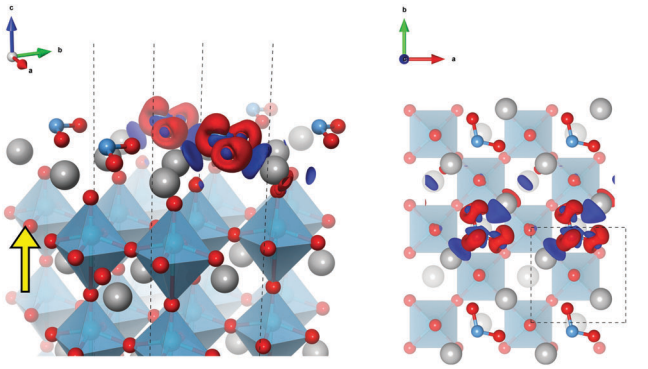

Fig. 21 Electron transfer from the Pb conduction band to the NO_2 LUMO on the positively poled PTO surface (0.5 ML coverage). N is shown in pale blue, O (red), Pb (gray) and Ti (Cyan). The yellow arrow shows the direction of ferroelectric polarization. A side view is shown on the left, and a top view is depicted on the right hand side. Regions of space which electrons migrate to are indicated by red while blue indicates the region which electrons migrate from upon adsorption of 0.5 ML NO_2.

Table 10 shows the polarization dependent interaction between methane and stoichiometric Pb-terminated PTO. We see that the positively poled reducing surface does not interact with CH_4 while the negatively poled oxidizing surface interacts strongly with CH_4 and oxidizes it to CH_3OH. We compute the energy barrier for this reaction (using the constrained relaxation method) to be $\approx$1.1 eV. The binding energy of CH_3OH to the remaining surface (with 0.5 ML O vacancy) is calculated to be negligible ($<$0.1 eV) and it can desorb very easily. Thus, one might think that a PTO surface with cycled polarization can convert CH_4 and O_2 to CH_3OH.

In principle, there are two problems that might hinder the cycle described above: (a) the produced CH_3OH in negative polarization might dissociate back to CH_4 and O on the reducing positively polarized surface, and (b) the unstable surface oxygens on negatively poled surface might find kinetically more favorable pathways to leave the surface. We have investigated both of these potential challenges. Regarding the first problem, CH_3OH prefers (by 1.6 eV per molecule) to dissociate back to CH_4 + O on the reducing positively polarized surface (the intact

Table 10 Polarization dependent binding energies for CH_4 and O_2 on stoichiometric Pb terminated $PbTiO_3$. The oxidizing negatively poled surface interacts strongly with CH_4 (forming CH_3OH), while the reducing positively poled surface interacts strongly with oxygen molecules (dissociating O_2 into adsorbed oxygen adatoms). The binding energy of CH_3OH to the remainder of the surface (with 0.5 ML O vacancy) is calculated to be negligible and it can desorb easily. Energies are relative to the molecules (CH_4 and O_2) in gas phase

Polarization	CH_4 binding energy (eV)	O_2 binding energy (eV)
Positive	0.0 (intact)	2.6 (dissociated)
Paraelectric	0.0 (intact)	0.2 (intact)
Negative	1.7* (forming CH_3OH)	0.0 (intact)

binding energy is calculated to be 0.4 eV while the dissociated binding energy for CH_4 + O is 2.0 eV). However, the dissociation barrier is $\approx$2.0 eV which means that although thermodynamics favors CH_3OH to dissociate back to CH_4 + O on the positive surface, the kinetics inhibits this reaction compared to the barrierless O_2 dissociation process which oxidizes and stabilizes the surface. Regarding the second problem, unfortunately, the kinetics hinders our plan. On the negatively poled surface, while the surface oxygens can oxidize methane to methanol (1.1 eV barrier per oxygen), they can instead directly pair up with their neighboring oxygen to form O_2 which leaves the surface (only 0.4 eV barrier per association event). Hence, it is unlikely the surface oxygen in the negatively poled case will actually oxidize any significant fraction of the methane.

Thus this simplest scheme of using polarization cycling of bare ferroelectric PTO to partially oxidize CH_4 into CH_3OH turns out to be unlikely due to unfavorable kinetics. However, there is still room for future research on this subject. One strategy, mentioned above, is to use monolayers of transition metal oxides on ferroelectric supports.[34,36,117] Here, one can still switch the surface between the oxidizing and reducing modes *via* polarization modulation while searching for a transition metal oxide monolayer that increases the direct O_2 formation barrier for negative polarization. This is a potentially rewarding optimization problem since it might unveil the first efficient direct partial oxidation process for methane.

4. Conclusions

We studied the electronic structure of the Pb terminated $PbTiO_3$ (PTO) surface as a function of polarization. We investigated the mechanism behind the surface reconstructions by analysis in electronic structure level using Density Functional Theory (DFT). It was shown that by using ferroelectric oxide surfaces, one can effectively convert SO_2 to SO_3 which is an important reaction for industrial production of sulfuric acid. We also described the polarization dependent surface chemistry of NO, NO_2, N_2, and O_2 molecules in both dissociated and intact binding modes. We discovered that the polarization can be used as a switch to control the binding energies of most of these species and showed that using a cycle of positive and negative (or paraelectric) polarizations can overcome the oxygen inhibition problem which has been a stumbling block for developing a NO_x direct decomposition catalyst (an open challenge in automotive emission control industry[279–283]). The only limitation of this scheme when using the bare PTO surface is that NO decomposition only happens at lower coverages ($\leq$0.25 ML). One can overcome this shortcoming by using systems in which the PTO surface is terminated with a monolayer of active transition metal oxide: such surfaces are more challenging to fabricate experimentally but promise functionality at higher coverages.[34] Finally, the possibility of using ferroelectrics to achieve partial oxidation of methane to methanol was investigated, and the results pointed to potential future research in this direction.

This work provides an example of how ferroelectrics under cyclic polarization conditions can help one go beyond the limits of the Sabatier principle.[33–36] A distinct observation, which may be explored in future work, is the breaking of symmetry between the electronic structure of the transition state and dissociated state of NO on positively polarized PTO. This can possibly lead to a method to break away from the scaling relations that impose fundamental limitations on the surface catalytic activity.

Acknowledgements

We thank Victor E. Henrich, Jens K. Norskov, Annabella Selloni, Eric I. Altman, Alexie M. Kolpak, Kevin G. Garrity, Andrew Sherman, Matthew Herdiech, Kimber Stamm Masias and Paul T. Fanson for inspiration and valuable discussions. This work was supported by the Toyota Research Institute of North America. Partial support for Ismail-Beigi was provided by NSF MRSEC DMR 1119826. Computational facilities were supported by NSF Grant No. CNS 08-21132 and by the facilities and staff of the Yale University Faculty of Arts and Sciences High Performance Computing Center. Additional computations were carried out *via* the NSF XSEDE resources through Grant No. TG-MCA08X007.

References

1 F. Studt, F. Abild-Pedersen, T. Bligaard, R. Z. Sorensen, C. H. Christensen and J. K. Norskov, *Science*, 2008, **320**, 1320–1322.
2 P. Ferrin, D. Simonetti, S. Kandoi, E. Kunkes, J. A. Dumesic, J. K. Norskov and M. Mavrikakis, *J. Am. Chem. Soc.*, 2009, **131**, 5809–5815.
3 F. Besenbacher, I. Chorkendorff, B. S. Clausen, B. Hammer, A. M. Molenbroek, J. K. Norskov and I. Stensgaard, *Science*, 1998, **279**, 1913–1915.
4 J. Greeley, I. E. L. Stephens, A. S. Bondarenko, T. P. Johansson, H. A. Hansen, T. F. Jaramillo, J. Rossmeisl, I. Chorkendorff and J. K. Norskov, *Nat. Chem.*, 2009, **1**, 552–556.
5 J. W. Erisman, M. A. Sutton, J. Galloway, Z. Klimont and W. Winiwarter, *Nat. Geosci.*, 2008, **1**, 636–639.
6 A. Hellman, K. Honkala, I. N. Remediakis, A. Logadottir, A. Carlsson, S. Dahl, C. H. Christensen and J. K. Norskov, *Surf. Sci.*, 2006, **600**, 4264–4268.
7 A. Vojvodic, A. J. Medford, F. Studt, F. Abild-Pedersen, T. S. Khan, T. Bligaard and J. K. Norskov, *Chem. Phys. Lett.*, 2014, **598**, 108–112.
8 A. J. Medford, A. Vojvodic, J. S. Hummelshoj, J. Voss, F. Abild-Pedersen, F. Studt, T. Bligaard, A. Nilsson and J. K. Norskov, *J. Catal.*, 2015, **328**, 36–42.
9 A. Vojvodic and J. K. Norskov, *Natl. Sci. Rev.*, 2015, nwv023.
10 J. K. Norskov, T. Bligaard, B. Hvolbek, F. Abild-Pedersen, I. Chorkendorff and C. H. Christensen, *Chem. Soc. Rev.*, 2008, **37**, 2163.
11 C. J. H. Jacobsen, S. Dahl, B. S. Clausen, S. Bahn, A. Logadottir and J. K. Norskov, *J. Am. Chem. Soc.*, 2001, **123**, 8404–8405.

12 M. P. Andersson, T. Bligaard, A. Kustov, K. E. Larsen, J. Greeley, T. Johannessen, C. H. Christensen and J. K. Norskov, *J. Catal.*, 2006, **239**, 501–506.
13 J. H. Montoya, C. Tsai, A. Vojvodic and J. K. Norskov, *ChemSusChem*, 2015, **8**, 2180–2186.
14 A. Logadottir, T. H. Rod, J. K. Norskov, B. Hammer, S. Dahl and C. J. H. Jacobsen, *J. Catal.*, 2001, **197**, 229–231.
15 A. Vojvodic, A. Hellman, C. Ruberto and B. I. Lundqvist, *Phys. Rev. Lett.*, 2009, **103**, 146103.
16 I. C. Man, H.-Y. Su, F. Calle-Vallejo, H. A. Hansen, J. I. Martínez, N. G. Inoglu, J. Kitchin, T. F. Jaramillo, J. K. Nørskov and J. Rossmeisl, *ChemCatChem*, 2011, **3**, 1159–1165.
17 A. Vojvodic, J. K. Norskov and F. Abild-Pedersen, *Top. Catal.*, 2013, **57**, 25–32.
18 Y. Wang, J. H. Montoya, C. Tsai, M. S. G. Ahlquist, J. K. Norskov and F. Studt, *Catal. Lett.*, 2015, **146**, 304–308.
19 S. Wang, *et al.*, *Phys. Chem. Chem. Phys.*, 2011, **13**, 20760.
20 A. Vojvodic, F. Calle-Vallejo, W. Guo, S. Wang, A. Toftelund, F. Studt, J. I. Martínez, J. Shen, I. C. Man, J. Rossmeisl, T. Bligaard, J. K. Norskov and F. Abild-Pedersen, *J. Chem. Phys.*, 2011, **134**, 244509.
21 E. M. Fernandez, P. G. Moses, A. Toftelund, H. A. Hansen, J. I. Martínez, F. Abild-Pedersen, J. Kleis, B. Hinnemann, J. Rossmeisl, T. Bligaard and J. K. Norskov, *Angew. Chem., Int. Ed.*, 2008, **47**, 4683–4686.
22 H. A. Hansen, J. B. Varley, A. A. Peterson and J. K. Nørskov, *J. Phys. Chem. Lett.*, 2013, **4**, 388–392.
23 J. S. Yoo, F. Abild-Pedersen, J. K. Norskov and F. Studt, *ACS Catal.*, 2014, **4**, 1226–1233.
24 M. M. Montemore and J. W. Medlin, *Catal. Sci. Technol.*, 2014, **4**, 3748–3761.
25 S. Siahrostami, H. Falsig, P. Beato, P. G. Moses, J. K. Nørskov and F. Studt, *ChemCatChem*, 2016, **8**, 767–772.
26 C. Tsai, *et al.*, *Catal. Lett.*, 2016, **146**, 718–724.
27 A. B. Laursen, I. C. Man, O. L. Trinhammer, J. Rossmeisl and S. Dahl, *J. Chem. Educ.*, 2011, **88**, 1711–1715.
28 R. R. Chianelli, G. Berhault, P. Raybaud, S. Kasztelan, J. Hafner and H. Toulhoat, *Appl. Catal., A*, 2002, **227**, 83–96.
29 N. B. Halck, V. Petrykin, P. Krtil and J. Rossmeisl, *Phys. Chem. Chem. Phys.*, 2014, **16**, 13682.
30 X. Hong, K. Chan, C. Tsai and J. K. Nørskov, *ACS Catal.*, 2016, 4428–4437.
31 Y. Li and Q. Sun, *Adv. Energy Mater.*, 2016, DOI: 10.1002/aenm.201600463.
32 H. A. Hansen, C. Shi, A. C. Lausche, A. A. Peterson and J. K. Nørskov, *Phys. Chem. Chem. Phys.*, 2016, **18**, 9194–9201.
33 A. Kakekhani, S. Ismail-Beigi and E. I. Altman, *Surf. Sci.*, 2015, **650**, 302–316.
34 A. Kakekhani and S. Ismail-Beigi, *ACS Catal.*, 2015, **5**, 4537–4545.
35 A. Kakekhani and S. Ismail-Beigi, *J. Mater. Chem. A*, 2016, **4**, 5235–5246.
36 B. O. Alawode and A. M. Kolpak, *J. Phys. Chem. Lett.*, 2016, **7**, 1310–1314.
37 G. Parravano, *J. Chem. Phys.*, 2004, **20**, 342–343.
38 Y. Inoue, I. Yoshioka and K. Sato, *J. Phys. Chem.*, 1984, **88**, 1148–1151.
39 Y. Inoue, M. Matsukawa and K. Sato, *J. Am. Chem. Soc.*, 1989, **111**, 8965–8966.
40 Y. Inoue and Y. Watanabe, *Catal. Today*, 1993, **16**, 487–494.
41 K. Garrity, A. M. Kolpak, S. Ismail-Beigi and E. I. Altman, *Adv. Mater.*, 2010, **22**, 2969–2973.
42 Z. Zhang, R. Gonzalez, G. Diaz, L. G. Rosa, I. Ketsman, X. Zhang, P. Sharma, A. Gruverman and P. A. Dowben, *J. Phys. Chem. C*, 2011, **115**, 13041–13046.
43 M. Sakar, S. Balakumar, P. Saravanan and S. Bharathkumar, *Nanoscale*, 2016, **8**, 1147–1160.
44 H. J. Lee, S.-H. Shin, K. T. Nam, J. Nah and M. H. Lee, *J. Mater. Chem. A*, 2016, **4**, 3223–3227.
45 R. Su, Y. Shen, L. Li, D. Zhang, G. Yang, C. Gao and Y. Yang, *Small*, 2015, **11**, 202–207.
46 L. Li, P. A. Salvador and G. S. Rohrer, *Nanoscale*, 2014, **6**, 24–42.
47 Y. Inoue, K. Sato, K. Sato and H. Miyama, *Chem. Phys. Lett.*, 1986, **129**, 79–81.
48 J. L. Giocondi and G. S. Rohrer, *J. Phys. Chem. B*, 2001, **105**, 8275–8277.
49 Y. Zhang, A. M. Schultz, P. A. Salvador and G. S. Rohrer, *J. Mater. Chem.*, 2011, **21**, 4168.
50 M. Stock and S. Dunn, *J. Phys. Chem. C*, 2012, **116**, 20854–20859.
51 M. A. Khan, M. A. Nadeem and H. Idriss, *Surf. Sci. Rep.*, 2016, **71**, 1–31.
52 Y. Cui, J. Briscoe and S. Dunn, *Chem. Mater.*, 2013, **25**, 4215–4223.
53 C. R. Bowen, H. A. Kim, P. M. Weaver and S. Dunn, *Energy Environ. Sci.*, 2014, **7**, 25–44.
54 Q. Liu, Y. Zhou, L. You, J. Wang, M. Shen and L. Fang, *Appl. Phys. Lett.*, 2016, **108**, 022902.
55 H. Li, Y. Sang, S. Chang, X. Huang, Y. Zhang, R. Yang, H. Jiang, H. Liu and Z. L. Wang, *Nano Lett.*, 2015, **15**, 2372–2379.
56 W. Yang, Y. Yu, M. B. Starr, X. Yin, Z. Li, A. Kvit, S. Wang, P. Zhao and X. Wang, *Nano Lett.*, 2015, **15**, 7574–7580.
57 D. Tiwari and S. Dunn, *J. Mater. Sci.*, 2009, **44**, 5063–5079.
58 Y. Cui, S. M. Goldup and S. Dunn, *RSC Adv.*, 2015, **5**, 30372–30379.
59 K. Chen, X. Huang, Y. Liu, M. Qi, Y. Hou, Y. Li, Y. Liang, X. Wang, W. Li and Q. Zhao, *Chem. Phys. Lett.*, 2015, **627**, 82–86.
60 T. Zhang, W. Lei, P. Liu, J. A. Rodriguez, J. Yu, Y. Qi, G. Liu and M. Liu, *Chem. Sci.*, 2015, **6**, 4118–4123.
61 J. J. Glickstein, P. A. Salvador and G. S. Rohrer, *J. Phys. Chem. C*, 2016, **120**, 12673–12684.
62 M. R. Morris, S. R. Pendlebury, J. Hong, S. Dunn and J. R. Durrant, *Adv. Mater.*, 2016, DOI: 10.1002/adma.201601238.
63 D. Fan, J. Zhu, X. Wang, S. Wang, Y. Liu, R. Chen, Z. Feng, F. Fan and C. Li, *ACS Appl. Mater. Interfaces*, 2016, **8**, 13857–13864.
64 X. Bai, J. Wei, B. Tian, Y. Liu, T. Reiss, N. Guiblin, P. Gemeiner, B. Dkhil and I. C. Infante, *J. Phys. Chem. C*, 2016, **120**, 3595–3601.

65 S. Kappadan, T. W. Gebreab, S. Thomas and N. Kalarikkal, *Mater. Sci. Semicond. Process.*, 2016, **51**, 42–47.
66 A. Alkeisy, L. Ren, D. Cui, Z. Xu, X. Xu, X. Su, W. Hao, S. X. Dou and Y. Du, *J. Mater. Chem. A*, 2016, DOI: 10.1039/C6TA03578G.
67 C. Paillard, X. Bai, I. C. Infante, M. Guennou, G. Geneste, M. Alexe, J. Kreisel and B. Dkhil, *Adv. Mater.*, 2016, DOI: 10.1002/adma.201505215.
68 Z. Fan, K. Sun and J. Wang, *J. Mater. Chem. A*, 2015, **3**, 18809–18828.
69 D.-F. Pan, G.-F. Bi, G.-Y. Chen, H. Zhang, J.-M. Liu, G.-H. Wang and J.-G. Wan, *Sci. Rep.*, 2016, DOI: 10.1038/srep22948.
70 S. B. Jo, M. Kim, D. H. Sin, J. Lee, H. G. Kim, H. Ko and K. Cho, *Adv. Energy Mater.*, 2015, DOI: 10.1002/aenm.201500802.
71 D. Li, M. H. Zhao, J. Garra, A. M. Kolpak, A. M. Rappe, D. A. Bonnell and J. M. Vohs, *Nat. Mater.*, 2008, **7**, 473–477.
72 Y. Yun and E. I. Altman, *J. Am. Chem. Soc.*, 2007, **129**, 15684–15689.
73 Y. Yun, L. Kampschulte, M. Li, D. Liao and E. I. Altman, *J. Phys. Chem. C*, 2007, **111**, 13951–13956.
74 J. Garra, J. M. Vohs and D. A. Bonnell, *Surf. Sci.*, 2009, **603**, 1106–1114.
75 M. H. Zhao, D. A. Bonnell and J. M. Vohs, *Surf. Sci.*, 2008, **602**, 2849–2855.
76 M. H. Zhao, D. A. Bonnell and J. M. Vohs, *Surf. Sci.*, 2009, **603**, 284–290.
77 S. Sanna, R. Hölscher and W. G. Schmidt, *Phys. Rev. B: Condens. Matter Mater. Phys.*, 2012, **86**, 205407.
78 A. Riefer, S. Sanna and W. G. Schmidt, *Phys. Rev. B: Condens. Matter Mater. Phys.*, 2012, **86**, 125410.
79 C. Braun, S. Sanna and W. G. Schmidt, *J. Phys. Chem. C*, 2015, **119**, 9342–9346.
80 D. Conklin, T.-H. Park, S. Nanayakkara, M. J. Therien and D. A. Bonnell, *Adv. Funct. Mater.*, 2011, **21**, 4712–4718.
81 S. V. Kalinin, D. A. Bonnell, T. Alvarez, X. Lei, Z. Hu, R. Shao and J. H. Ferris, *Adv. Mater.*, 2004, **16**, 795–799.
82 D. Li and D. A. Bonnell, *Ceram. Int.*, 2008, **34**, 157–164.
83 A. Nguyen, P. Sharma, T. Scott, E. Preciado, V. Klee, D. Sun, I.-H. D. Lu, D. Barroso, S. Kim, V. Y. Shur, A. R. Akhmatkhanov, A. Gruverman, L. Bartels and P. A. Dowben, *Nano Lett.*, 2015, **15**, 3364–3369.
84 C. R. Bowen, J. Taylor, E. LeBoulbar, D. Zabek, A. Chauhan and R. Vaish, *Energy Environ. Sci.*, 2014, **7**, 3836–3856.
85 X. Li, S.-G. Lu, X.-Z. Chen, H. Gu, X.-s. Qian and Q. M. Zhang, *J. Mater. Chem. C*, 2013, **1**, 23–37.
86 C. R. Bowen, R. Stevens, L. J. Nelson, A. C. Dent, G. Dolman, B. Su, T. W. Button, M. G. Cain and M. Stewart, *Smart Mater. Struct.*, 2006, **15**, 295.
87 J. Briscoe and S. Dunn, *Nanostructured Piezoelectric Energy Harvesters*, SpringerBriefs in Materials, Springer International Publishing, 2014, pp. 3–17, DOI: 10.1007/978-3-319-09632-2_2.
88 D. Guyomar, G. Sebald, S. Pruvost, M. Lallart, A. Khodayari and C. Richard, *J. Intell. Mater. Syst. Struct.*, 2009, **20**, 609–624.
89 N. Nuraje and K. Su, *Nanoscale*, 2013, **5**, 8752–8780.
90 A. R. Damodaran, J. C. Agar, S. Pandya, Z. Chen, L. Dedon, R. Xu, B. Apgar, S. Saremi and L. W. Martin, *J. Phys.: Condens. Matter*, 2016, **28**, 263001.
91 C. Ederer and N. A. Spaldin, *Phys. Rev. Lett.*, 2005, **95**, 257601.
92 M. B. Kelman, P. C. McIntyre, B. C. Hendrix, S. M. Bilodeau and J. F. Roeder, *J. Appl. Phys.*, 2003, **93**, 9231–9236.
93 Y. Zhang, J. Hong, B. Liu and D. Fang, *Nanotechnology*, 2010, **21**, 015701.
94 J. X. Zhang, D. G. Schlom, L. Q. Chen and C. B. Eom, *Appl. Phys. Lett.*, 2009, **95**, 122904.
95 D. G. Schlom, L.-Q. Chen, C.-B. Eom, K. M. Rabe, S. K. Streiffer and J.-M. Triscone, *Annu. Rev. Mater. Res.*, 2007, **37**, 589–626.
96 H. Lu, C.-W. Bark, D. E. d. l. Ojos, J. Alcala, C. B. Eom, G. Catalan and A. Gruverman, *Science*, 2012, **336**, 59–61.
97 S. Liu, Y. Kim, L. Z. Tan and A. M. Rappe, *Nano Lett.*, 2016, **16**, 1663–1668.
98 D. Lee, A. Yoon, S. Y. Jang, J.-G. Yoon, J.-S. Chung, M. Kim, J. F. Scott and T. W. Noh, *Phys. Rev. Lett.*, 2011, **107**, 057602.
99 J. Wu, W. Mao, Z. Wu, X. Xu, H. You, A. Xue and Y. Jia, *Nanoscale*, 2016, **8**, 7343–7350.
100 H. Lin, Z. Wu, Y. Jia, W. Li, R.-K. Zheng and H. Luo, *Appl. Phys. Lett.*, 2014, **104**, 162907.
101 A. Benke, E. Mehner, M. Rosenkranz, E. Dmitrieva, T. Leisegang, H. Stöcker, W. Pompe and D. C. Meyer, *J. Phys. Chem. C*, 2015, **119**, 18278–18286.
102 E. Gutmann, A. Benke, K. Gerth, H. Böttcher, E. Mehner, C. Klein, U. Krause-Buchholz, U. Bergmann, W. Pompe and D. C. Meyer, *J. Phys. Chem. C*, 2012, **116**, 5383–5393.
103 K.-S. Hong, H. Xu, H. Konishi and X. Li, *J. Phys. Chem. C*, 2012, **116**, 13045–13051.
104 K.-S. Hong, H. Xu, H. Konishi and X. Li, *J. Phys. Chem. Lett.*, 2010, **1**, 997–1002.
105 M. B. Starr, J. Shi and X. Wang, *Angew. Chem., Int. Ed.*, 2012, **51**, 5962–5966.
106 M. B. Starr and X. Wang, *Sci. Rep.*, 2013, **3**, 2160, DOI: 10.1038/srep02160.
107 M. B. Starr and X. Wang, *Nano Energy*, 2015, **14**, 296–311.
108 Y.-T. Wang and K.-S. Chang, *J. Am. Ceram. Soc.*, 2016, DOI: 10.1111/jace.14264.
109 M.-K. Lo, S.-Y. Lee and K.-S. Chang, *J. Phys. Chem. C*, 2015, **119**, 5218–5224.
110 G. Cravotto and P. Cintas, *Chem. Sci.*, 2012, **3**, 295–307.
111 A. M. Kolpak, I. Grinberg and A. M. Rappe, *Phys. Rev. Lett.*, 2007, **98**, 166101.
112 S. V. Levchenko and A. M. Rappe, *Phys. Rev. Lett.*, 2008, **100**, 256101.
113 Y. Mi, G. Geneste, J. E. Rault, C. Mathieu, A. Pancotti and N. Barrett, *J. Phys.: Condens. Matter*, 2012, **24**, 275901.
114 J. H. Lee and A. Selloni, *Phys. Rev. Lett.*, 2014, **112**, 196102.
115 R. Holscher, W. G. Schmidt and S. Sanna, *J. Phys. Chem. C*, 2014, **118**, 10213–10220.
116 P. Chen, Y. Xu, N. Wang, A. R. Oganov and W. Duan, *Phys. Rev. B: Condens. Matter Mater. Phys.*, 2015, **92**, 085432.

117 K. Garrity, A. Kakekhani, A. Kolpak and S. Ismail-Beigi, *Phys. Rev. B: Condens. Matter Mater. Phys.*, 2013, **88**, 045401.
118 S. Sanna, C. Dues and W. G. Schmidt, *Comput. Mater. Sci.*, 2015, **103**, 145–150.
119 S. Sanna, C. Thierfelder, S. Wippermann, T. P. Sinha and W. G. Schmidt, *Phys. Rev. B: Condens. Matter Mater. Phys.*, 2011, **83**, 054112.
120 R. V. Wang, D. D. Fong, F. Jiang, M. J. Highland, P. H. Fuoss, C. Thompson, A. M. Kolpak, J. A. Eastman, S. K. Streiffer, A. M. Rappe and G. B. Stephenson, *Phys. Rev. Lett.*, 2009, **102**, 047601.
121 E. Cook, *Nature*, 1926, **117**, 419–421.
122 K.-H. Dorr, H. Grimm, W. Weber, M. Tacke, G. Schmidt, Process for producing sulfuric acid, 1977; U.S. Classification 423/522, 423/531, 95/235; International Classification C01B17/775; Cooperative Classification C01B17/775; European Classification C01B17/775.
123 M. Muehlhofer, T. Strassner and W. A. Herrmann, *Angew. Chem., Int. Ed.*, 2002, **41**, 1745–1747.
124 J. H. Lunsford, *Catal. Today*, 2000, **63**, 165–174.
125 R. Palkovits, M. Antonietti, P. Kuhn, A. Thomas and F. Schuth, *Angew. Chem., Int. Ed.*, 2009, **48**, 6909–6912.
126 M. Soorholtz, R. J. White, T. Zimmermann, M.-M. Titirici, M. Antonietti, R. Palkovits and F. Schuth, *Chem. Commun.*, 2013, **49**, 240–242.
127 S. Impeng, P. Khongpracha, C. Warakulwit, B. Jansang, J. Sirijaraensre, M. Ehara and J. Limtrakul, *RSC Adv.*, 2014, **4**, 12572.
128 M. C. Alvarez-Galvan, N. Mota, M. Ojeda, S. Rojas, R. M. Navarro and J. L. G. Fierro, *Catal. Today*, 2011, **171**, 15–23.
129 H. D. Gesser, N. R. Hunter and C. B. Prakash, *Chem. Rev.*, 1985, **85**, 235–244.
130 C. Hammond, S. Conrad and I. Hermans, *ChemSusChem*, 2012, **5**, 1668–1686.
131 A. Holmen, *Catal. Today*, 2009, **142**, 2–8.
132 S. Murcia-Lopez, K. Villa, T. Andreu and J. R. Morante, *ACS Catal.*, 2014, **4**, 3013–3019.
133 R. Raja and P. Ratnasamy, *Appl. Catal., A*, 1997, **158**, L7–L15.
134 Z.-J. Zhao, A. Kulkarni, L. Vilella, J. K. Nørskov and F. Studt, *ACS Catal.*, 2016, **6**, 3760–3766.
135 P. P. Knops-Gerrits and W. A. Goddard III, *J. Mol. Catal. A: Chem.*, 2001, **166**, 135–145.
136 M. Dawber, K. M. Rabe and J. F. Scott, *Rev. Mod. Phys.*, 2005, **77**, 1083–1130.
137 J. F. Scott, *Science*, 2007, **315**, 954–959.
138 M. T. Buscaglia, V. Buscaglia, M. Viviani, P. Nanni and M. Hanuskova, *J. Eur. Ceram. Soc.*, 2000, **20**, 1997–2007.
139 J. Iniguez and L. Bellaiche, *Phys. Rev. Lett.*, 2001, **87**, 095503.
140 J. P. Attfield, *Cryst. Eng.*, 2002, **5**, 427–438.
141 J. P. Attfield, *Int. J. Inorg. Mater.*, 2001, **3**, 1147–1152.
142 D. Li and M. A. Subramanian, *Solid State Sci.*, 2000, **2**, 507–512.
143 S. Datta, M. Rioult, D. Stanescu, H. Magnan and A. Barbier, *Thin Solid Films*, 2016, **607**, 7–13.
144 J. Rogal, K. Reuter and M. Scheffler, *Phys. Rev. B: Condens. Matter Mater. Phys.*, 2004, **69**, 075421.
145 K. Reuter and M. Scheffler, *Phys. Rev. Lett.*, 2003, **90**, 046103.
146 K. Reuter, C. Stampf and M. Scheffler, in *Handbook of Materials Modeling*, ed. S. Yip, Springer Netherlands, 2005, pp. 149–194, DOI: 10.1007/978-1-4020-3286-8_10.
147 K. Reuter and M. Scheffler, *Appl. Phys. A: Mater. Sci. Process.*, 2004, **78**, 793–798.
148 B. Meyer, J. Padilla and D. Vanderbilt, *Faraday Discuss.*, 1999, **114**, 395–405.
149 A. Munkholm, S. K. Streiffer, M. V. Ramana Murty, J. A. Eastman, C. Thompson, O. Auciello, L. Thompson, J. F. Moore and G. B. Stephenson, *Phys. Rev. Lett.*, 2001, **88**, 016101.
150 D. D. Fong, A. M. Kolpak, J. A. Eastman, S. K. Streiffer, P. H. Fuoss, G. B. Stephenson, C. Thompson, D. M. Kim, K. J. Choi, C. B. Eom, I. Grinberg and A. M. Rappe, *Phys. Rev. Lett.*, 2006, **96**, 127601.
151 P. Gao, H.-J. Liu, Y.-L. Huang, Y.-H. Chu, R. Ishikawa, B. Feng, Y. Jiang, N. Shibata, E.-G. Wang and Y. Ikuhara, *Nat. Commun.*, 2016, **7**, 11318.
152 J. M. Vohs and M. A. Barteau, *Surf. Sci.*, 1988, **201**, 481–502.
153 J. M. Vohs and M. A. Barteau, *Surf. Sci.*, 1986, **176**, 91–114.
154 Y. Bai, W. Zhang, Z. Zhang, J. Zhou, X. Wang, C. Wang, W. Huang, J. Jiang and Y. Xiong, *J. Am. Chem. Soc.*, 2014, **136**, 14650–14653.
155 S. Bai, M. Xie, Q. Kong, W. Jiang, R. Qiao, Z. Li, J. Jiang and Y. Xiong, *Part. Part. Syst. Charact.*, 2016, DOI: 10.1002/ppsc.201500239.
156 S. Bai, C. Wang, M. Deng, M. Gong, Y. Bai, J. Jiang and Y. Xiong, *Angew. Chem., Int. Ed.*, 2014, **53**, 12120–12124.
157 T. Kittel and E. Roduner, *J. Phys. Chem. C*, 2016, DOI: 10.1021/acs.jpcc.6b00899.
158 T. Kittel and E. Roduner, *J. Phys. Chem. C*, 2016, DOI: 10.1021/acs.jpcc.6b00898.
159 S. Bai, L. Yang, C. Wang, Y. Lin, J. Lu, J. Jiang and Y. Xiong, *Angew. Chem.*, 2015, **127**, 15023–15027.
160 X. Li, W. Zhong, P. Cui, J. Li and J. Jiang, *J. Phys. Chem. Lett.*, 2016, **7**, 1750–1755.
161 P. Gorai, E. G. Seebauer and E. Ertekin, *J. Chem. Phys.*, 2016, **144**, 184708.
162 J. Sołtys, J. Piechota, M. opuszyński and S. Krukowski, *J. Cryst. Growth*, 2013, **374**, 53–59.
163 N. Z. Koocher, D. Saldana-Greco, F. Wang, S. Liu and A. M. Rappe, *J. Phys. Chem. Lett.*, 2015, **6**, 4371–4378.
164 L. An, H. Yan, X. Chen, B. Li, Z. Xia and D. Xia, *Nano Energy*, 2016, **20**, 134–143.
165 Y. Bai, C. Wang, X. Zhou, J. Lu and Y. Xiong, *Prog. Nat. Sci.: Mater. Int.*, 2016, DOI: 10.1016/j.pnsc.2016.05.010.
166 C. Wang, S. Bai and Y. Xiong, *Chin. J. Catal.*, 2015, **36**, 1476–1493.
167 C. Ederer and N. A. Spaldin, *Phys. Rev. B: Condens. Matter Mater. Phys.*, 2006, **74**, 020401.
168 C. Ederer and N. A. Spaldin, *Nat. Mater.*, 2004, **3**, 849–851.
169 E. Salje, *Ferroelectrics*, 1990, **104**, 111–120.

170 D. Lee, S. H. Baek, T. H. Kim, J.-G. Yoon, C. M. Folkman, C. B. Eom and T. W. Noh, *Phys. Rev. B: Condens. Matter Mater. Phys.*, 2011, **84**, 125305.
171 D. Cao, Z. Wang, Nasori, L. Wen, Y. Mi and Y. Lei, *Angew. Chem.*, 2014, **126**, 11207–11211.
172 Z. Fan, W. Ji, T. Li, J. Xiao, P. Yang, K. P. Ong, K. Zeng, K. Yao and J. Wang, *Acta Mater.*, 2015, **88**, 83–90.
173 J. L. Wang, B. L. Liu, X. L. Zhao, B. B. Tian, Y. H. Zou, S. Sun, H. Shen, J. L. Sun, X. J. Meng and J. H. Chu, *Appl. Phys. Lett.*, 2014, **104**, 182907.
174 Y. Lu, J. Claude, B. Neese, Q. Zhang and Q. Wang, *J. Am. Chem. Soc.*, 2006, **128**, 8120–8121.
175 D. A. Bonnell, *Science*, 2013, **339**, 401–402.
176 X.-M. Jiang, Z.-B. Yan, D. Liu, J.-X. Wang, M.-F. Liu, G.-C. Guo, B.-B. Jin, X.-G. Li and J.-M. Liu, *Chem. – Asian J.*, 2013, **8**, 2925–2931.
177 Z. Cui, K. Gao, C. Liu, Y. Yin, D.-W. Fu, H.-L. Cai and X. S. Wu, *J. Phys. Chem. C*, 2016, **120**, 2925–2931.
178 P. Hohenberg and W. Kohn, *Phys. Rev.*, 1964, **136**, B864–B871.
179 W. Kohn and L. J. Sham, *Phys. Rev.*, 1965, **140**, A1133–A1138.
180 P. Giannozzi, *et al.*, *J. Phys.: Condens. Matter*, 2009, **21**, 395502.
181 K. Laasonen, R. Car, C. Lee and D. Vanderbilt, *Phys. Rev. B: Condens. Matter Mater. Phys.*, 1991, **43**, 6796–6799.
182 D. Vanderbilt, *Phys. Rev. B: Condens. Matter Mater. Phys.*, 1990, **41**, 7892–7895.
183 K. Laasonen, A. Pasquarello, R. Car, C. Lee and D. Vanderbilt, *Phys. Rev. B: Condens. Matter Mater. Phys.*, 1993, **47**, 10142–10153.
184 L. Bengtsson, *Phys. Rev. B: Condens. Matter Mater. Phys.*, 1999, **59**, 12301–12304.
185 N. Marzari, D. Vanderbilt, A. De Vita and M. C. Payne, *Phys. Rev. Lett.*, 1999, **82**, 3296–3299.
186 J. P. Perdew and W. Yue, *Phys. Rev. B: Condens. Matter Mater. Phys.*, 1986, **33**, 8800–8802.
187 J. P. Perdew, K. Burke and Y. Wang, *Phys. Rev. B: Condens. Matter Mater. Phys.*, 1996, **54**, 16533–16539.
188 M. S. J. Marshall, A. Malashevich, A. S. Disa, M.-G. Han, H. Chen, Y. Zhu, S. Ismail-Beigi, F. J. Walker and C. H. Ahn, *Phys. Rev. Appl.*, 2014, **2**, 051001.
189 A. M. Kolpak, D. Li, R. Shao, A. M. Rappe and D. A. Bonnell, *Phys. Rev. Lett.*, 2008, **101**, 036102.
190 G. Mills and H. Jónsson, *Phys. Rev. Lett.*, 1994, **72**, 1124–1127.
191 G. Mills, H. Jonsson and G. K. Schenter, *Surf. Sci.*, 1995, **324**, 305–337.
192 G. Henkelman and H. Jónsson, *J. Chem. Phys.*, 2000, **113**, 9978–9985.
193 G. Henkelman, B. P. Uberuaga and H. Jonsson, *J. Chem. Phys.*, 2000, **113**, 9901–9904.
194 A. Alavi, P. Hu, T. Deutsch, P. L. Silvestrelli and J. Hutter, *Phys. Rev. Lett.*, 1998, **80**, 3650–3653.
195 L. M. Molina and B. Hammer, *Phys. Rev. B: Condens. Matter Mater. Phys.*, 2004, **69**, 155424.
196 D. G. Truhlar, B. C. Garrett and S. J. Klippenstein, *J. Phys. Chem.*, 1996, **100**, 12771–12800.
197 I. M. Ciobîcâ, F. Frechard, R. A. van Santen, A. W. Kleyn and J. Hafner, *J. Phys. Chem. B*, 2000, **104**, 3364–3369.
198 R. D. King-Smith and D. Vanderbilt, *Phys. Rev. B: Condens. Matter Mater. Phys.*, 1993, **47**, 1651–1654.
199 D. Vanderbilt and R. D. King-Smith, *Phys. Rev. B: Condens. Matter Mater. Phys.*, 1993, **48**, 4442–4455.
200 T. Morita and Y. Cho, *Jpn. J. Appl. Phys.*, 2004, **43**, 6535.
201 H. Morioka, G. Asano, T. Oikawa, H. Funakubo and K. Saito, *Appl. Phys. Lett.*, 2003, **82**, 4761–4763.
202 S. Sanna, R. Holscher and W. G. Schmidt, *Appl. Surf. Sci.*, 2014, **301**, 70–78.
203 D. G. Popescu, M. A. Husanu, L. Trupina, L. Hrib, L. Pintilie, A. Barinov, S. Lizzit, P. Lackvig and C. M. Teodorescu, *Phys. Chem. Chem. Phys.*, 2015, **17**, 509–520.
204 A. Wander, F. Schedin, P. Steadman, A. Norris, R. McGrath, T. S. Turner, G. Thornton and N. M. Harrison, *Phys. Rev. Lett.*, 2001, **86**, 3811–3814.
205 J. M. Carlsson, *Comput. Mater. Sci.*, 2001, **22**, 24–31.
206 C. Baeumer, D. Saldana-Greco, J. M. P. Martirez, A. M. Rappe, M. Shim and L. W. Martin, *Nat. Commun.*, 2015, **6**, 6136.
207 J. M. P. Martirez, E. H. Morales, W. A. Saidi, D. A. Bonnell and A. M. Rappe, *Phys. Rev. Lett.*, 2012, **109**, 256802.
208 D. Lee, B. C. Jeon, A. Yoon, Y. J. Shin, M. H. Lee, T. K. Song, S. D. Bu, M. Kim, J.-S. Chung, J.-G. Yoon and T. W. Noh, *Adv. Mater.*, 2014, **26**, 5005–5011.
209 P. Ágoston, K. Albe, R. M. Nieminen and M. J. Puska, *Phys. Rev. Lett.*, 2009, **103**, 245501.
210 R. J. Farrauto and R. M. Heck, *Catal. Today*, 1999, **51**, 351–360.
211 P. Brijesh and S. Sreedhara, *Int. J. Automot. Technol.*, 2013, **14**, 195–206.
212 Y. Nagao, Y. Nakahara, T. Sato, H. Iwakura, S. Takeshita, S. Minami, H. Yoshida and M. Machida, *ACS Catal.*, 2015, **5**, 1986–1994.
213 M. Haneda, T. Kaneko, N. Kamiuchi and M. Ozawa, *Catal. Sci. Technol.*, 2015, **5**, 1792–1800.
214 M. A. van Spronsen, G. J. C. van Baarle, C. T. Herbschleb, J. W. M. Frenken and I. M. N. Groot, *Catal. Today*, 2015, **244**, 85–95.
215 J. Wang, H. Chen, Z. Hu, M. Yao and Y. Li, *Catal. Rev.*, 2015, **57**, 79–144.
216 M. Ozawa, T. Okouchi and M. Haneda, *Catal. Today*, 2015, **242**(Part B), 329–337.
217 G. Beulertz, M. Votsmeier and R. Moos, *Appl. Catal., B*, 2015, **165**, 369–377.
218 K. Roy and C. S. Gopinath, *ChemCatChem*, 2014, **6**, 531–537.
219 A. Sabbaghi, F. L. Y. Lam and X. Hu, *Appl. Catal., A*, 2015, **508**, 25–36.
220 R. You, Y. Zhang, D. Liu, M. Meng, Z. Jiang, S. Zhang and Y. Huang, *Chem. Eng. J.*, 2015, **260**, 357–367.
221 N. Imanaka and T. Masui, *Appl. Catal., A*, 2012, **431–432**, 1–8.
222 H. Falsig, T. Bligaard, J. Rass-Hansen, A. L. Kustov, C. H. Christensen and J. K. Norskov, *Top. Catal.*, 2007, **45**, 117–120.
223 A. Amirnazmi, J. E. Benson and M. Boudart, *J. Catal.*, 1973, **30**, 55–65.
224 S. S. C. Chuang and C.-D. Tan, *J. Phys. Chem. B*, 1997, **101**, 3000–3004.

225 C. Tofan, D. Klvana and J. Kirchnerova, *Appl. Catal., A*, 2002, **223**, 275–286.
226 C. Tofan, D. Klvana and J. Kirchnerova, *Appl. Catal., A*, 2002, **226**, 225–240.
227 M. W. Herdiech, X. Zhu, M. D. Morales-Acosta, F. J. Walker and E. I. Altman, *Phys. Chem. Chem. Phys.*, 2015, **17**, 9488–9498.
228 J. L. Falconer and J. A. Schwarz, *Catal. Rev.*, 1983, **25**, 141–227.
229 K. Momma and F. Izumi, *J. Appl. Crystallogr.*, 2011, **44**, 1272–1276.
230 H. Orita, I. Nakamura and T. Fujitani, *J. Chem. Phys.*, 2005, **122**, 014703.
231 D. Loffreda, D. Simon and P. Sautet, *J. Catal.*, 2003, **213**, 211–225.
232 H. Aizawa, Y. Morikawa, S. Tsuneyuki, K. Fukutani and T. Ohno, *Surf. Sci.*, 2002, **514**, 394–403.
233 J. Beheshtian, M. Kamfiroozi, Z. Bagheri and A. Ahmadi, *Phys. E*, 2011, **44**, 546–549.
234 X.-R. Shi, J. Wang and K. Hermann, *J. Phys. Chem. C*, 2010, **114**, 13630–13641.
235 W. Zhang, Z. Li, Y. Luo and J. Yang, *J. Chem. Phys.*, 2008, **129**, 134708.
236 P. J. Feibelman and D. R. Hamann, *Phys. Rev. Lett.*, 1984, **52**, 61–64.
237 N. Inoglu and J. R. Kitchin, *Phys. Rev. B: Condens. Matter Mater. Phys.*, 2010, **82**, 045414.
238 S. E. Mason, I. Grinberg and A. M. Rappe, *J. Phys. Chem. B*, 2006, **110**, 3816–3822.
239 J. J. Mortensen, B. Hammer and J. K. Norskov, *Surf. Sci.*, 1998, **414**, 315–329.
240 P.-O. Lowdin, *J. Chem. Phys.*, 1950, **18**, 365–375.
241 A. Kokalj, *J. Mol. Graphics Modell.*, 1999, **17**, 176–179.
242 I. Nakamura, T. Fujitani and H. Hamada, *Surf. Sci.*, 2002, **514**, 409–413.
243 H. Jiang, L. Xing, O. Czuprat, H. Wang, S. Schirrmeister, T. Schiestel and J. Caro, *Chem. Commun.*, 2009, 6738.
244 H. Jiang, H. Wang, F. Liang, S. Werth, T. Schiestel and J. Caro, *Angew. Chem., Int. Ed.*, 2009, **48**, 2983–2986.
245 Y. Li and W. K. Hall, *J. Catal.*, 1991, **129**, 202–215.
246 M. Haneda and H. Hamada, *C. R. Chim.*, DOI: 10.1016/j.crci.2015.07.016.
247 A. L. Allred, *J. Inorg. Nucl. Chem.*, 1961, **17**, 215–221.
248 R. P. Iczkowski and J. L. Margrave, *J. Am. Chem. Soc.*, 1961, **83**, 3547–3551.
249 X. Duan, O. Warschkow, A. Soon, B. Delley and C. Stampfl, *Phys. Rev. B: Condens. Matter Mater. Phys.*, 2010, **81**, 075430.
250 M. Todorova, K. Reuter and M. Scheffler, *J. Phys. Chem. B*, 2004, **108**, 14477–14483.
251 M. V. Ganduglia-Pirovano and M. Scheffler, *Phys. Rev. B: Condens. Matter Mater. Phys.*, 1999, **59**, 15533–15543.
252 C. Stampfl and M. Scheffler, *Phys. Rev. B: Condens. Matter Mater. Phys.*, 1996, **54**, 2868–2872.
253 W.-X. Li, C. Stampfl and M. Scheffler, *Phys. Rev. B: Condens. Matter Mater. Phys.*, 2002, **65**, 075407.
254 J. R. Kitchin, *Phys. Rev. B: Condens. Matter Mater. Phys.*, 2009, **79**, 205412.
255 M. Mavrikakis, B. Hammer and J. K. Nørskov, *Phys. Rev. Lett.*, 1998, **81**, 2819–2822.
256 B. Hammer and J. K. Norskov, *Nature*, 1995, **376**, 238–240.
257 B. Hammer, *Top. Catal.*, 2006, **37**, 3–16.
258 B. Hammer, L. B. Hansen and J. K. Norskov, *Phys. Rev. B: Condens. Matter Mater. Phys.*, 1999, **59**, 7413–7421.
259 S. H. Ma, Z. Y. Jiao and Z. X. Yang, *Surf. Sci.*, 2010, **604**, 817–823.
260 S. H. Ma, Z. Y. Jiao, T. X. Wang and X. Q. Dai, *Surf. Sci.*, 2014, **619**, 90–97.
261 S. H. Ma, Z. Y. Jiao, X. Q. Dai and Z. X. Yang, *Eur. Phys. J. B*, 2011, **83**, 437–443.
262 H. Zhang, A. Soon, B. Delley and C. Stampfl, *Phys. Rev. B: Condens. Matter Mater. Phys.*, 2008, **78**, 045436.
263 S. D. Miller and J. R. Kitchin, *Surf. Sci.*, 2009, **603**, 794–801.
264 P. Kaghazchi and T. Jacob, *Phys. Rev. B: Condens. Matter Mater. Phys.*, 2011, **83**, 035417.
265 S. Starschich, S. Menzel and U. Böttger, *Appl. Phys. Lett.*, 2016, **108**, 032903.
266 L. Chen, Z. Cheng, W. Xu, X. Meng, G. Yuan, J. Liu and Z. Liu, *Sci. Rep.*, 2016, **6**, 19092, DOI: 10.1038/srep19092.
267 A. Lipatov, P. Sharma, A. Gruverman and A. Sinitskii, *ACS Nano*, 2015, **9**, 8089–8098.
268 C. Wang, K.-j. Jin, Z.-t. Xu, L. Wang, C. Ge, H.-b. Lu, H.-z. Guo, M. He and G.-z. Yang, *Appl. Phys. Lett.*, 2011, **98**, 192901.
269 A. Chernikova, M. Kozodaev, A. Markeev, D. Negrov, M. Spiridonov, S. Zarubin, O. Bak, P. Buragohain, H. Lu, E. Suvorova, A. Gruverman and A. Zenkevich, *ACS Appl. Mater. Interfaces*, 2016, **8**, 7232–7237.
270 C. Ko, Y. Lee, Y. Chen, J. Suh, D. Fu, A. Suslu, S. Lee, J. D. Clarkson, H. S. Choe, S. Tongay, R. Ramesh and J. Wu, *Adv. Mater.*, 2016, **28**, 2923–2930.
271 P. Ponath, K. Fredrickson, A. B. Posadas, Y. Ren, X. Wu, R. K. Vasudevan, M. Baris Okatan, S. Jesse, T. Aoki, M. R. McCartney, D. J. Smith, S. V. Kalinin, K. Lai and A. A. Demkov, *Nat. Commun.*, 2015, **6**, 6067.
272 Y. Cao, Q. Li, L.-Q. Chen and S. V. Kalinin, *Appl. Phys. Lett.*, 2015, **107**, 202905.
273 J. P. Velev, J. D. Burton, M. Y. Zhuravlev and E. Y. Tsymbal, *npj Comput. Mater.*, 2016, **2**, 16009, DOI: 10.1038/npjcompumats.2016.9.
274 J. Y. Jo, H. S. Han, J.-G. Yoon, T. K. Song, S.-H. Kim and T. W. Noh, *Phys. Rev. Lett.*, 2007, **99**, 267602.
275 J. Y. Jo, D. J. Kim, Y. S. Kim, S.-B. Choe, T. K. Song, J.-G. Yoon and T. W. Noh, *Phys. Rev. Lett.*, 2006, **97**, 247602.
276 B. Hammer and J. K. Norskov, in *Impact of Surface Science on Catalysis*, ed. H. K. Bruce and C. Gates, Advances in Catalysis, Academic Press, 2000, vol. 45, pp. 71–129.
277 A. Eichler and J. Hafner, *Phys. Rev. Lett.*, 1997, **79**, 4481–4484.
278 A. Eichler and J. Hafner, *Phys. Rev. B: Condens. Matter Mater. Phys.*, 1999, **59**, 5960–5967.
279 S. Matsumoto, *Catal. Today*, 2004, **90**, 183–190.
280 E. Jobson, *Top. Catal.*, 2004, **28**, 191–199.
281 M. V. Twigg, *Appl. Catal., B*, 2007, **70**, 2–15.
282 P. Granger and V. I. Parvulescu, *Chem. Rev.*, 2011, **111**, 3155–3207.
283 Z.-P. Liu and P. Hu, *Top. Catal.*, 2004, **28**, 71–78.